We thank Referee #1 for his/her comments on our paper, which helped us to improve the quality of the paper. Below, we answer the reviewer's question point by point.

General comments

This paper reported the development of an incoherent broadband cavity enhanced absorption spectrometer for simultaneous measurement of NO_2, glyoxal (GLY) and methylglyoxal (MGLY). A NO_2 photolytic convertor (NPC) was used to minimize the interference of high concentration NO_2 to GLY. The photolysis of NO_2 can lead to the formation of O_3. My major comment is that if the photolysis of ambient air can potentially generate artificial GLY or MGLY, especially in VOCs rich environments.

Reply:

Given the size of the photolysis cell (i.e., a cylinder with 60 mm length and 13.4 mm inner diameter) and the sampling flow rate of 2 L/min, the residence time of the sampled air in the cell is about 0.25 s. In such a short period, the production of GLY and MGLY in the cell is negligible which can be verified by model simulations. The model includes the full MCM chemistry (version 3.3.1, http://mcm.leeds.ac.uk/MCM/) for all NMHCs and their oxidation products. The initial concentrations of OH, HO_2, O_3, NO, HONO, CO, CH_4, C_2-C_{12} NMHCs are set to the average values obtained during a field observation campaign in 2018 in Yangtze River Delta, China (Table S1). The total OH reactivity due to NMHCs is about 3.1 s^{-1}. The relative humidity, temperature, and pressure are constrained by the campaign averages, i.e., 60%, 300 K, 1007.65 hPa, respectively. The photolysis frequencies are constrained by values calculated from the spectral actinic flux inside the cell (Fig. S1). The spectral actinic flux is estimated by the LED emission spectrum and by the concentration change of NO, NO_2, and O_3 when NO_2 standard (100 ppb) is running through the system. The initial values of NO_2, GLY, MGLY are set to 60 ppb, 100 ppt, and 100 ppt, respectively. Fig. S2 shows the calculated concentrations of NO_2, O_3, GLY, and MGLY for the period of 0.25 s residence time. While the NO_2 concentration drops from 60 ppb to 15 ppb leading to an increase of O_3 concentration by approximately 45 ppb, the change of GLY and MGLY concentrations is only around 1%. As shown in Fig. S3, the production rate of GLY and MGLY increases to around 5 ppb h^{-1} which could only result in maximumly 0.34 ppt increase of GLY and MGLY. Even if we increase the initial NMHCs concentration in the model by a factor of 10, the maximum production of GLY and MGLY within 250 ms is less than 2 ppt which is only 2% of their initial concentration (Fig. S4). Since the NMHCs concentration in the model represents typical atmospheric condition influenced by urban air pollution, our model simulation clearly shows that the NPC can be used in the field observations for removing NO_2 without additional production of GLY and MGLY.

The above discussions are added in the Supplement.

Specific comments

1, page 2, line 17. A careful survey of GLY instruments is encouraged. A short discussion about recent IBBCEAS systems used for GLY measurements and their detection limits is better than only a sentence of other gas's applications.

Reply:

The following texts are added on page 2, line 24 in the revised manuscript.

"Washenfelder et al. were the first to use this technology to measure GLY. The precision (1σ) of their system is 29 ppt for a 1 min sampling time (Washenfelder et al., 2008). Under the same time resolution, Thalman and Volkamer reduced the detection limit (2σ) to 19 ppt for their LED-CE-DOAS (Thalman and Volkamer, 2010). The above two systems have been successfully applied to GLY measurements in field observations (Washenfelder et al., 2011; Coburn et al., 2014). From aspects of miniaturization and improving time resolution, Min et al. optimized Washenfelder et al.'s IBBCEAS for aircraft GLY measurements. The measurement precision (2σ) is 34 ppt in 5 s (Min et al., 2016). The IBBCEAS developed by Fang et al. has a precision of 28 ppt for GLY at 1 min averaging time. By applying Kalman filter to the retrieved concentrations, their measurement precision was improved to 8 ppt in 21 s (Fang et al., 2017). "

2, page 2, line 28. I note a paper recently accepted for publication in AMT that also tried to fix the problem of NO_2 interference to GLY, which should be included in the introduction.

Liang, S., Qin, M., Xie, P., Duan, J., Fang, W., He, Y., Xu, J., Tang, K., Meng, F., Ye, K., Liu, J., and Liu, W.: Development of an incoherent broadband cavity-enhanced absorption spectrometer for measurements of ambient glyoxal and NO_2 in a polluted urban environment, Atmos. Meas. Tech. Discuss., https://doi.org/10.5194/amt-2018-430, in review, 2018.

Reply:

The following texts are added in page 2, line 28 in the revised manuscript.

"Liang et al. thought that the interference was caused by the accuracy of the convoluted NO_2 absorption cross section and tried to solve this problem by measuring NO_2 cross section with their own spectrometer (Liang et al., 2019). In this case, the accuracy of the retrieved NO_2 and GLY concentrations will be dependent on the accuracy of the NO_2 cross section they measured. "

3, page 5. How to determine the absolute GLY concentration in this work is still not clear, by measuring the pressure or flow rate?

Reply:

The absolution concentration of GLY is determined by fitting the reference spectra of NO_2, GLY, MGLY, etc. to the measured absorption coefficient, according to equations 1 and 2 in Page 5. We also measure the pressure and the temperature in the cavity of the IBBCEAS, so that the absolute concentration can be converted to mixing ratio. In this work, the absolute concentration of GLY in the NO_2 photolytic converter is determined by the IBBCEAS system. For checking the influence of NPC on the GLY sampling efficiency, we only need to look at the relative change of the measured GLY concentration.

4, page 7, line 19. The relative change of 1-R is more meaningful than R.

Reply:

We revise the text according to your suggestion.

5, page 11, sec. 4.2. Please include the fitting residual information and give some discussion about the "unknown reasons". Did the authors shift or stretch the reference spectrum?

Reply:

We did apply shift and stretch on the reference spectra. The shift was limited within -1 nm to 1 nm and the stretch was limited within 0.9 to 1.1. The following texts are added in Sect. 4.2.

"…The fitting residual increased from 4×10^{-10} to 2×10^{-9} as the NO_2 concentration increased…. The uncertainty of simulation results is mainly caused by two reasons. (1) Random numbers could be not good enough to represent the actual noise of the whole system. Since the intensity of LED and the reflectivity of mirrors are not evenly distributed with the wavelength, the corresponding signal-to-noise ratios (SNR) are also different at different wavelength. As for our system, the SNR within 450-468 nm are higher than that at other wavelengths. If we only reduced the random number by 5 times within 450-468 nm and did not change that at other wavelengths, the fluctuation of the fitted GLY concentration was also reduced by 5 times. (2) The impact of Rayleigh scattering and Mie scattering are not explicitly considered during the simulation. In this case, whether polynomial should be added in the spectral fitting or not would be a problem. The retrieved GLY concentration by using a fifth-order polynomial was 20% higher than that without including polynomial. Therefore…."

6, page 12, sec. 4.4. Please include the comparisons with other IBBCEAS systems. The sensitivity of Min et al.'s was 1.5x10ˆ-10 cm-1, and the authors' was 8.4x10ˆ-11 cm- 1 (with 100 s integration time, line 18 in the text). Table 2 is not clear (5s, 100s). The corresponding time for each detection limit needs to be clearly stated. Furthermore, please carefully check if the data used in Table 2 are correct.

Reply:

The second paragraph in Sect. 4.4 is rewritten in the revised manuscript.

According to figure 8 in Min et al. (2016), we estimated the Allan deviation of their system for a 100 s acquisition time as 1.5×10^{-10} cm^{-1} (2σ). With respect to its GLY detect limitation, it was given in as 5 s average in Min et al.'s paper. We carefully checked the data used in Table 2 and made necessary revisions.

7, page 23, Fig. 4, please check the convolution of MGL reference is correct. There is an obvious shift, and the peaks are vanished.

Reply:

Thank you for pointing out this mistake. We tested two high resolution cross sections of MGLY at the very beginning of our experiments, one is from Meller et al. (1991) and the other is from Staffelbach et al. (1995). In the manuscript, we mistook convolution results based on Staffelbach's spectrum instead of that based on Meller's spectrum. We revised Fig. 4 accordingly and checked the whole manuscript to ensure that the correct cross section is used in every part involving MGLY spectral fitting.

8, page 27, Fig. 8(a). The symbols are not clearly indicated.
Reply:
Revised accordingly in the manuscript.

Reference

Meller, R., Raber, W., Crowley, J. N., Jenkin, M. E., and Moortgat, G. K.: THE UV-VISIBLE ABSORPTION-SPECTRUM OF METHYLGLYOXAL, Journal of Photochemistry and Photobiology a-Chemistry, 62, 163-171, 1991.

Min, K. E., Washenfelder, R. A., Dubé, W. P., Langford, A. O., Edwards, P. M., Zarzana, K. J., Stutz, J., Lu, K., Rohrer, F., Zhang, Y., and Brown, S. S.: A broadband cavity enhanced absorption spectrometer for aircraft measurements of glyoxal, methylglyoxal, nitrous acid, nitrogen dioxide, and water vapor, Atmos Meas Tech, 9, 423-440, 2016.

Staffelbach, T. A., Orlando, J. J., Tyndall, G. S., and Calvert, J. G.: THE UV-VISIBLE ABSORPTION-SPECTRUM AND PHOTOLYSIS QUANTUM YIELDS OF METHYLGLYOXAL, J Geophys Res-Atmos, 100, 14189-14198, 1995.

Table S1. Initial concentration of species included in the model simulation.

Species	Concentration	Species	Concentration
OH	107 cm-3	NO	0.60 ppb
HO2	109 cm-3	HONO	0.45 ppb
CH4	1.9 ppm	CO	0.33 ppm
O3	70.00 ppb	SO2	1.33 ppb
NO2	60 ppb	MGLY	100.0 ppt
GLY	100.0 ppt	TOLUENE	0.515 ppb
C2H2	1.000 ppb	NC8H18	0.034 ppb
CBUT2ENE	0.050 ppb	EBENZ	0.140 ppb
C2H4	0.900 ppb	MXYL	0.045 ppb
C2H6	2.130 ppb	NC9H20	0.019 ppb
IC4H10	0.380 ppb	OXYL	0.076 ppb
IC5H12	0.330 ppb	STYRENE	0.017 ppb
NC4H10	0.650 ppb	IPBENZ	0.012 ppb
NC5H12	0.240 ppb	PBENZ	0.014 ppb
PENT1ENE	0.004 ppb	METHTOL	0.016 ppb
TPENT2ENE	0.002 ppb	PETHTOL	0.015 ppb
C5H8	0.233 ppb	NC10H22	0.017 ppb
CPENT2ENE	0.003 ppb	TM135B	0.014 ppb
M22C4	0.019 ppb	OETHTOL	0.036 ppb
M23C4	0.020 ppb	TM123B	0.014 ppb
M2PE	0.100 ppb	PXYL	0.045 ppb
M3PE	0.076 ppb	NC11H24	0.019 ppb
HEX1ENE	0.009 ppb	C3H8	2.010 ppb
NC6H14	0.130 ppb	C3H6	0.120 ppb
M2HEX	0.030 ppb	C4H6	0.005 ppb
CHEX	0.044 ppb	TM124B	0.016 ppb
M3HEX	0.041 ppb	TBUT2ENE	0.002 ppb
BENZENE	0.364 ppb	BUT1ENE	0.040 ppb
NC7H16	0.055 ppb		

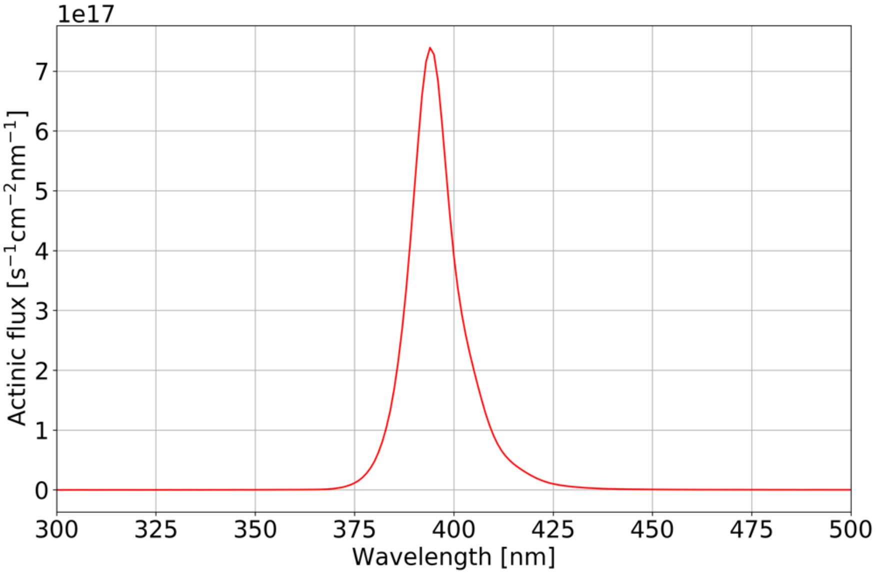

Figure S1. Spectral actinic flux inside the photolysis cell of the NO_2 convertor.

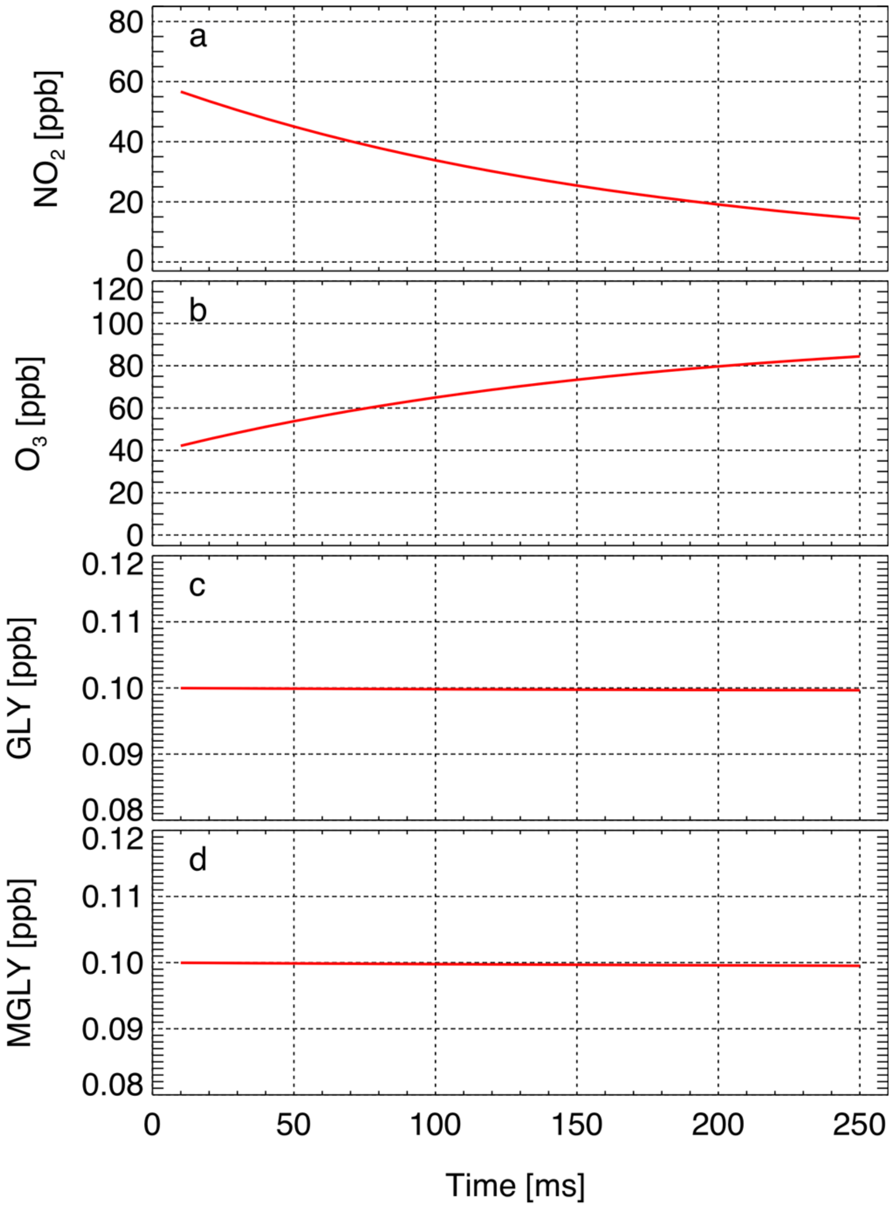

Figure S2. Model calculated concentrations of NO_2 (a), O_3 (b), GLY (c), and MGLY (d) in the photolysis cell of the NO_2 convertor. Note that the concentrations at 250 ms represent the condition of the sampled air exits the cell, since the residence time in the cell is about 250 ms.

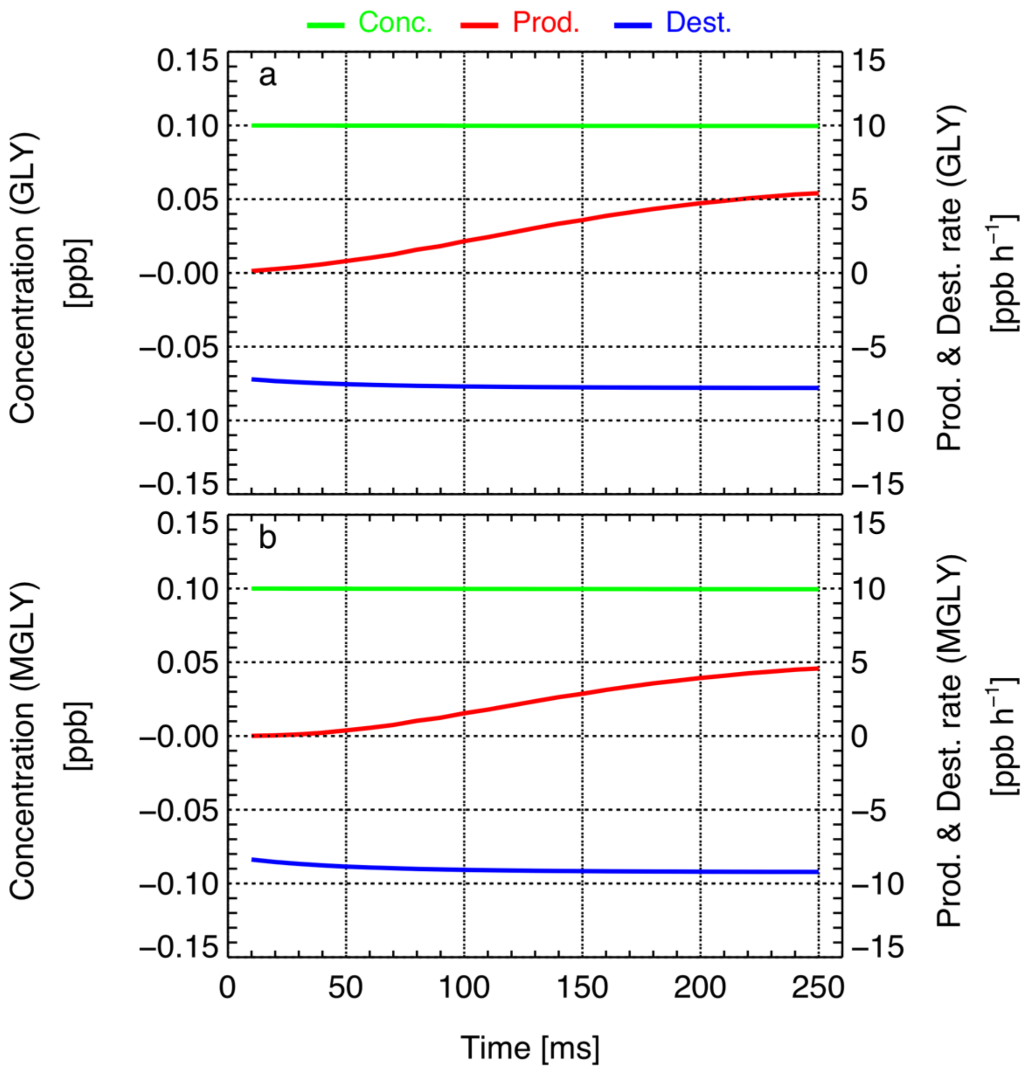

Figure S3. Model calculated concentrations (green), production rates (red), and destruction rates (blue) of GLY (a) and MGLY (b) in the photolysis cell of the NO_2 convertor. Note that the concentrations at 250 ms represent the condition of the sampled air exits the cell, since the residence time in the cell is about 250 ms.

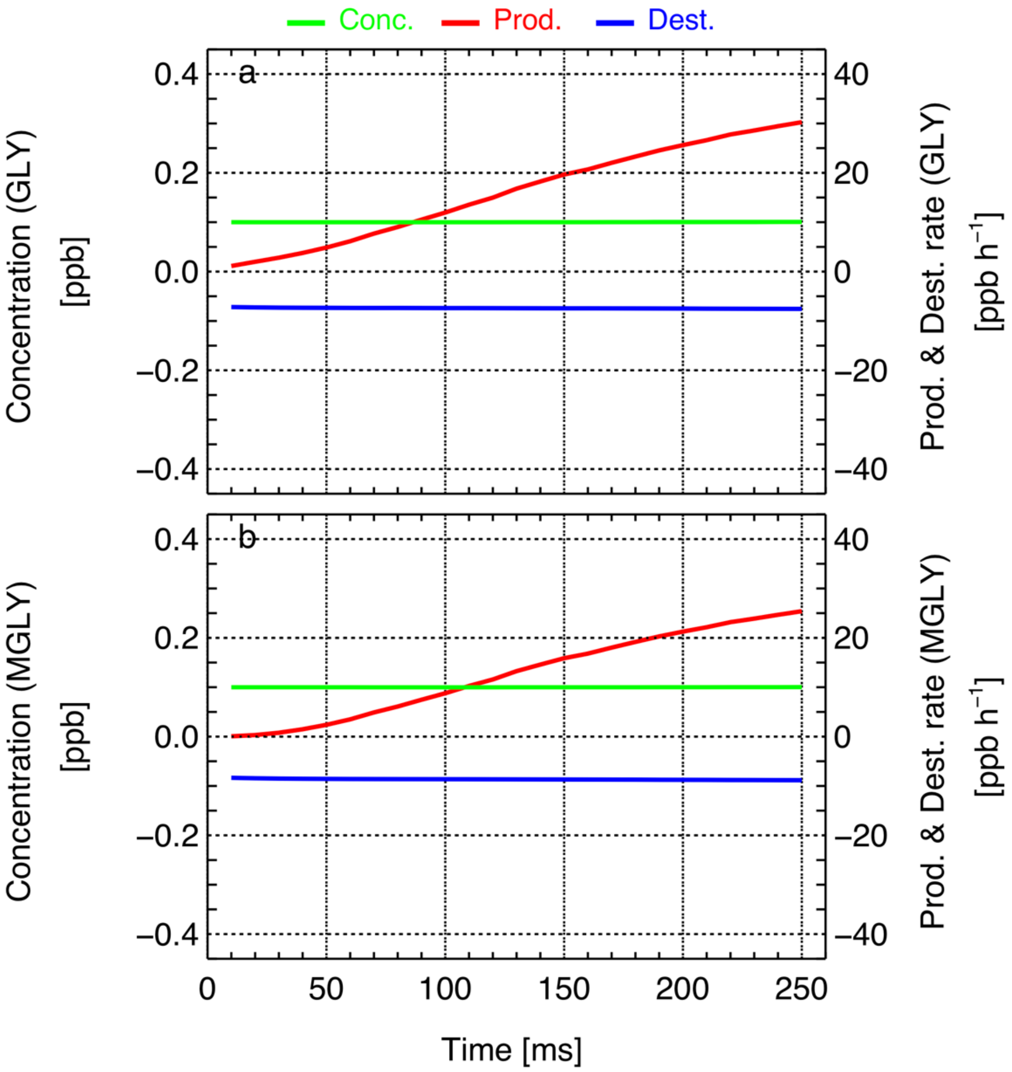

Figure S4. Model calculated concentration (green), production rate (red), and destruction rate (blue) of GLY (a) and MGLY (b) in the photolysis cell of the NO_2 converter. The initial concentrations of NMHCs in the model are set to 10 times of the values listed in Table 1. Note that the concentrations at 250 ms represent the condition of the sampled air exits the cell, since the residence time in the cell is about 250 ms.

We thank Referee #2 for his/her comments on our paper, which helped us to improve the quality of the paper. Below, we answer the reviewer's question point by point.

Liu et al. describe a new incoherent broadband cavity enhanced absorption spectrometer (IBBCEAS) for atmospheric measurements of NO_2, glyoxal, and methyl glyoxal. The instrument has been thoroughly characterized and performs well compared to existing methods. As a new feature, the instrument used a photolytic converter (NPC) to selectively reduce the amount of NO_2 in their sample stream. Major revisions will be required before this paper is acceptable for publication.

(1) There are too many figures in the current draft. Many are not necessary.

Reply:

We have revised the manuscript and the number of figures have been shorten to 10. Some figures which we think could be helpful for illustrating the performance of our IBBCEAS system are shown in the Supplement.

(2) Some figures are unclear as the captions are too short.

Reply:

Captions of all figures in the manuscript are revised in the way that clearly describing the figure content.

(3) I was not convinced of the merits of the NPC. Is the NPC even necessary? It seems that (valid) data could be obtained without it, though at a slightly higher noise level.

Reply:

At the beginning of the experiments, we have the same doubt as you about how much NPC can improve the quality of measurements. Subsequent experiments indicate that NPC not only reduces noise level, but also weakens the measuring interference of high NO_2 concentrations. As shown in Fig. 8(a) and (b) in the revised manuscript, the NO_2 concentrations reduced by 76% and GLY concentrations reduced by 5% when the NPC was turned on. With respect to well-mixed NO_2 and GLY, the concentration of NO_2 dropped rapidly while the NPC was running and the concentration of GLY increased. After the NPC turned off, the concentrations of the two compounds returned to the same level as before the NPC was turned on (Fig. 8c). So the concentration of GLY determined by IBBCEAS can be underestimated in the presence of high NO_2 concentrations and by utilizing NPC to reduce the NO_2 concentration, the measurement accuracy of GLY is improved.

(4) Does the NPC generate glyoxal and methyl glyoxal when ambient air containing organic compounds is sampled? The MCM lists 127 precursors for glyoxal and 143 precursors for methyl glyoxal. I haven't gone through these lists in detail, but it seems that more characterization experiments are warranted in my opinion. It seems to me that the NPC may generate more issues than it solves.

Reply:

Given the size of the photolysis cell (i.e., a cylinder with 60 mm length and 13.4 mm inner diameter) and the sampling flow rate of 2 L/min, the residence time of the sampled air in the cell is about 0.25 s. In such a short period, the production of GLY and MGLY in the cell is negligible which can be verified by model simulations. The model includes the full MCM chemistry (version 3.3.1, http://mcm.leeds.ac.uk/MCM/) for all NMHCs and their oxidation products. The initial concentrations of OH, HO_2, O_3, NO, HONO, CO, CH_4, C_2-C_{12} NMHCs are set to the average values obtained during a field observation campaign in 2018 in Yangtze River Delta, China (Table S1). The total OH reactivity due to NMHCs is about 20 s^{-1}. The relative humidity, temperature, and pressure are constrained by the campaign averages, i.e., 60%, 300 K, 1007.65 hPa, respectively. The photolysis frequencies are constrained by values calculated from the spectral actinic flux inside the cell (Fig. S1). The spectral actinic flux is estimated by the LED emission spectrum and by the concentration change of NO, NO_2, and O_3 when NO_2 standard (100 ppb) is running through the system. The initial values of NO_2, GLY, MGLY are set to 60 ppb, 100 ppt, and 100 ppt, respectively. Fig. S2 shows the calculated concentrations of NO_2, O_3, GLY, and MGLY for the period of 0.25 s residence time. While the NO_2 concentration drops from 60 ppb to 15 ppb leading to an increase of O_3 concentration by approximately 45 ppb, the change of GLY and MGLY concentrations is only around 1%. As shown in Fig. S3, the production rate of GLY and MGLY increases to around 5 ppb h^{-1} which could only result in maximumly 0.34 ppt increase of GLY and MGLY. Even if we increase the initial NMHCs concentration in the model by a factor of 10, the maximum production of GLY and MGLY within 250 ms is less than 2 ppt which is only 2% of their initial concentration (Fig. S4). Since the NMHCs concentration in the model represents typical atmospheric condition influenced by urban air pollution, our model simulation clearly shows that the NPC can be used in the field observations for removing NO_2 without additional production of GLY and MGLY.

The above discussions are added in the Supplement.

(5) The convolved spectrum of MGLY (Figure 4, thick purple line) does not look correct.

Reply:

Thank you for pointing out this mistake. We tested two high resolution cross sections of MGLY at the very beginning of our experiments, one is from Meller et al. (1991) and the other is from Staffelbach et al.(1995). In the manuscript, we mistook convolution results based on Staffelbach's spectrum instead of that based on Meller's spectrum. We revised Fig. 4 accordingly and checked the whole manuscript to ensure that the correct cross sections are used in every part involving MGLY spectral fitting.

Specific comments

pg 2, line 28 "Thalman et al. first encountered the challenge of fitting GLY and MGLY absorption spectra in the presence of high NO_2 concentrations (Thalman et al., 2015). To our knowledge, an effective method has not yet to solve this problem." This is a bit of mischaracterization - Thalman et al. [2015] stated that "For both CE-DOAS and BBCEAS ... we do not find significant bias; i.e., an upper-limit change in glyoxal due to

NO_2 is derived as +/-200 pptv glyoxal in the presence of 200 ppbv NO_2 (or bias of 1 pptv glyoxal/1 ppbv NO_2)."- see also major comment #3.

Reply:

According to Fig. 4 in Thalman et al. (2015), we can find that the fluctuation of the measured glyoxal concentration increased at least twice when NO_2 concentration reached 150 ppb. In addition, even though the upper-limit change in glyoxal due to NO_2 is derived as ±200 ppt glyoxal in the presence of 200 ppb NO_2 on the whole, the measurement interference on glyoxal already reached around 150 ppt when 50 ppb NO_2 was added. Since the ambient mixing ratios of glyoxal typically range between 10 ppt and 100 ppt, and NO_2 concentration in polluted area can reach 50 ppb or even higher, accurate quantification of glyoxal could be a challenge under this condition.

pg 7 line 31. Consider adding a digit to each uncertainty as otherwise 4% + 2% = 4%.

Reply:

Revised accordingly in the manuscript.

pg 9 line 23. "The presence of high NO_2 concentrations may affect the spectral fitting of GLY and MGLY". Perhaps, but this is not obvious from Figure 9 (which seem OK to me). To make their point, it seems like the authors could perform a rather easy experiment: Deliver a constant concentration of GLY (or MGLY) and add increasing amounts of NO_2 to this blend. Are the correct GLY (or MGLY) concentrations retrieved?

Reply:

Similar experiment as you suggested was performed in the Sect. 4.2. We delivered a constant concentration of GLY and add decreasing amounts of NO_2 to this blend for four times. The concentration of GLY measured by IBBCEAS increased as that of NO_2 decreased, although only the NO_2 concentration was reduced manually. The experimental phenomenon indicates that the presence of NO_2 will affect the retrieved concentration of GLY.

Figure 1 (a) Consider adding dimensions to this sketch, such as the inter-mirror distance

Reply:

Revised accordingly in the manuscript.

Figure 2 is not necessary in my opinion. Simply state the result in the text.

Reply:

Thank you for your advice. Figure 2 is deleted and corresponding results are stated in the text of the revised manuscript.

Figure 3. You may want to state the dimensions of the mixing chamber, temperature of the cold trap, and flow rates.

Reply:

Detailed information such as the dimensions of the mixing chamber is added to the caption of Figure 3. This figure is moved to the Supplement.

Figure 4 The convolved methylglyoxal spectrum does not look right.

Reply:

Revised accordingly in the manuscript.

Figure 6. This factor will be flow rate dependent, and the sample flow rate should be stated in the caption. Please zoom in on the ratio more (0.85 to 0.95) and state the standard deviation of this measurement. The effective path was determined from a comparison of measured to known concentration; the figure is misleading as it is suggested that it was determined by turning the purge gases on and off (filling the purge flow volumes would take much more time than shown here). Consider clarifying this in the text.

Reply:

Thank you for your advice. Figure 6 is re-plotted as you suggested and its caption is rewritten including sample flow rate and standard deviation of this measurement. This figure is moved to Supplement. The method of determining effective path that we used in the manuscript is measuring NO_2 concentration with or without purging flows. This kind of method has been approved by peers. For example, Duan et al. (2018) calculated the reduction of the effective cavity length successfully by measuring O_2-O_2 collision pair with or without purging flows.

Figure 11 The figure caption should describe the experiment conducted here in more detail. Figure 11 (c) The figure caption should indicate what is meant by the yellow overlay. Are the times displayed correct? It seems that the NO_2 mixing ratios stay at the high levels well after the NPC was turned on, but increase again before the NPC is turned off?

Reply:

The figure caption is rewritten as following and Figure 11 (c) is re-plotted.

"(a) NO_2 only test: A concentration gradient of NO_2 gas samples were measured twice, with the NPC on (yellow overlay) and off. The removal efficiency is constant at 76 % for different NO_2 concentrations. (b) GLY only test: The constant concentration of GLY produced by the standard gas generator was measured with the NPC on (yellow overlay) and off. A small fraction of the GLY (5%) was photolyzed by the NPC. (c) NO_2 and GLY mixture test: Well-mixed NO_2 and GLY was measured with the NPC on (yellow overlay) and off. The concentration of NO_2 dropped while the NPC was running and that of GLY increased. After the NPC was turned off, their concentrations returned to the same level as before the NPC was turned on."

Figure 12 - what does 'fixing' the concentration mean? What is 'first', 'second', 'third', and 'fourth'?

Reply:

The figure caption is rewritten as following.

"(a) Keep the concentration of GLY constant and mix it evenly with different concentrations of NO_2 for four times. The concentration of GLY measured by IBBCEAS increased as that of NO_2 decreased, although only the NO_2 concentration was reduced manually. (b) Simulate a series of spectra with constant GLY concentration and increasing NO_2 concentration and then calculate concentrations of GLY and NO_2 by retrieving these simulated spectra. The retrieved GLY concentration decreased with the increasing NO_2 concentration, although the set value of GLY concentration in the simulation was kept constant."

Figure 13 (b). There are two sets of concentrations displayed which one is methylglyoxal, and what is the other one?

Reply:

Both sets of concentrations displayed are methylglyoxal. The figure caption is rewritten as following. This figure is moved to Supplement.

"(a) Four spectral fit ranges (440-451 nm, 445-453 nm, 440-453 nm, and 430-453 nm) for MGLY. (b) Each spectral fit range was used to fit two experimental sets of MGLY produced by the standard gas generator. Experimental results of both sets indicated that fit range has a great influence on the fitted concentrations of MGLY."

Figure 14. The figure caption should indicate what is meant by the yellow overlay. (b) Are the times displayed correct? It seems that the NO_2 mixing ratios stay at the high levels well after the NPC was turned on, but increase again before the NPC is turned off? The photo-oxidation of certain organic molecules (e.g., benzene, toluene etc.) can yield glyoxal or methylglyoxal. It looks like this is happening here. Consider evaluating the NPC while sampling an atmospheric background of those VOCs.

Reply:

The figure caption is rewritten as following and Figure 14 (b) is re-plotted in the manuscript.

"(a) The constant concentration of MGLY produced by the standard gas generator was measured with the NPC on (yellow overlay) and off. The effect of NPC on MGLY concentration is negligible. (b) Well-mixed NO_2 and MGLY was measured with the NPC on (yellow overlay) and off. The concentration of NO_2 dropped while the NPC was running and that of MGLY increased. After the NPC was turned off, their concentrations returned to the same level as before the NPC was turned on."

The experimental results shown in Figure 14(b) are the concentration of measuring the mixture of methylglyoxal and NO_2. Because the gas mixture only contained methylglyoxal, NO_2, and N_2, the increase of methylglyoxal concentration cannot be caused by the photooxidation of certain organic molecules. So the methylglyoxal concentration determined by IBBCEAS could be underestimated and we used NPC to reduce the interference.

The advice of evaluating the NPC while sampling an atmospheric background of VOCs is reasonable. The results of model simulation shows that the production of GLY and MGLY in the NPC is negligible. For more information please refer to the reply of major comment (4).

Fig 14 (c) The caption does not adequately describe what is shown in the figure.

Reply:

The caption of Fig. 14(c) is rewritten as following.

"(c) Simulate a series of spectra with constant MGLY concentration and increasing NO_2 concentration and then calculate concentrations of MGLY and NO_2 by retrieving these simulated spectra. The retrieved MGLY concentration decreased with the increasing NO_2 concentration, although the set value of MGLY concentration in the simulation was kept constant."

Reference

Duan, J., Qin, M., Ouyang, B., Fang, W., Li, X., Lu, K., Tang, K., Liang, S., Meng, F., Hu, Z., Xie, P., Liu, W., and Häsler, R.: Development of an incoherent broadband cavity-enhanced absorption spectrometer for in situ measurements of HONO and NO2, Atmos Meas Tech, 11, 4531-4543, 2018.

Meller, R., Raber, W., Crowley, J. N., Jenkin, M. E., and Moortgat, G. K.: THE UV-VISIBLE ABSORPTION-SPECTRUM OF METHYLGLYOXAL, Journal of Photochemistry and Photobiology a-Chemistry, 62, 163-171, 1991.

Staffelbach, T. A., Orlando, J. J., Tyndall, G. S., and Calvert, J. G.: THE UV-VISIBLE ABSORPTION-SPECTRUM AND PHOTOLYSIS QUANTUM YIELDS OF METHYLGLYOXAL, J Geophys Res-Atmos, 100, 14189-14198, 1995.

Thalman, R., Baeza-Romero, M., Ball, S., Borrás, E., Daniels, M., Goodall, I., Henry, S., Karl, T., Keutsch, F., and Kim, S.: Instrument intercomparison of glyoxal, methyl glyoxal and NO2 under simulated atmospheric conditions, 2015. 2015.

Table S1. Initial concentration of species included in the model simulation.

Species	Concentration	Species	Concentration
OH	10^7 cm^{-3}	NO	0.60 ppb
HO2	10^9 cm^{-3}	HONO	0.45 ppb
CH4	1.9 ppm	CO	0.33 ppm
O3	70.00 ppb	SO2	1.33 ppb
NO2	60 ppb	MGLY	100.0 ppt
GLY	100.0 ppt	TOLUENE	0.515 ppb
C2H2	1.000 ppb	NC8H18	0.034 ppb
CBUT2ENE	0.050 ppb	EBENZ	0.140 ppb
C2H4	0.900 ppb	MXYL	0.045 ppb
C2H6	2.130 ppb	NC9H20	0.019 ppb
IC4H10	0.380 ppb	OXYL	0.076 ppb
IC5H12	0.330 ppb	STYRENE	0.017 ppb
NC4H10	0.650 ppb	IPBENZ	0.012 ppb
NC5H12	0.240 ppb	PBENZ	0.014 ppb
PENT1ENE	0.004 ppb	METHTOL	0.016 ppb
TPENT2ENE	0.002 ppb	PETHTOL	0.015 ppb
C5H8	0.233 ppb	NC10H22	0.017 ppb
CPENT2ENE	0.003 ppb	TM135B	0.014 ppb
M22C4	0.019 ppb	OETHTOL	0.036 ppb
M23C4	0.020 ppb	TM123B	0.014 ppb
M2PE	0.100 ppb	PXYL	0.045 ppb
M3PE	0.076 ppb	NC11H24	0.019 ppb
HEX1ENE	0.009 ppb	C3H8	2.010 ppb
NC6H14	0.130 ppb	C3H6	0.120 ppb
M2HEX	0.030 ppb	C4H6	0.005 ppb
CHEX	0.044 ppb	TM124B	0.016 ppb
M3HEX	0.041 ppb	TBUT2ENE	0.002 ppb
BENZENE	0.364 ppb	BUT1ENE	0.040 ppb
NC7H16	0.055 ppb		

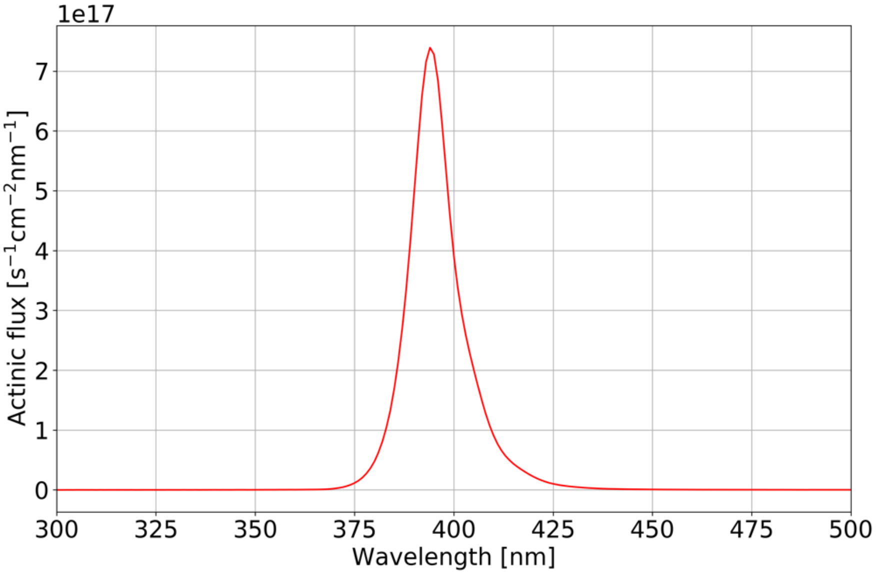

Figure S1. Spectral actinic flux inside the photolysis cell of the NO_2 convertor.

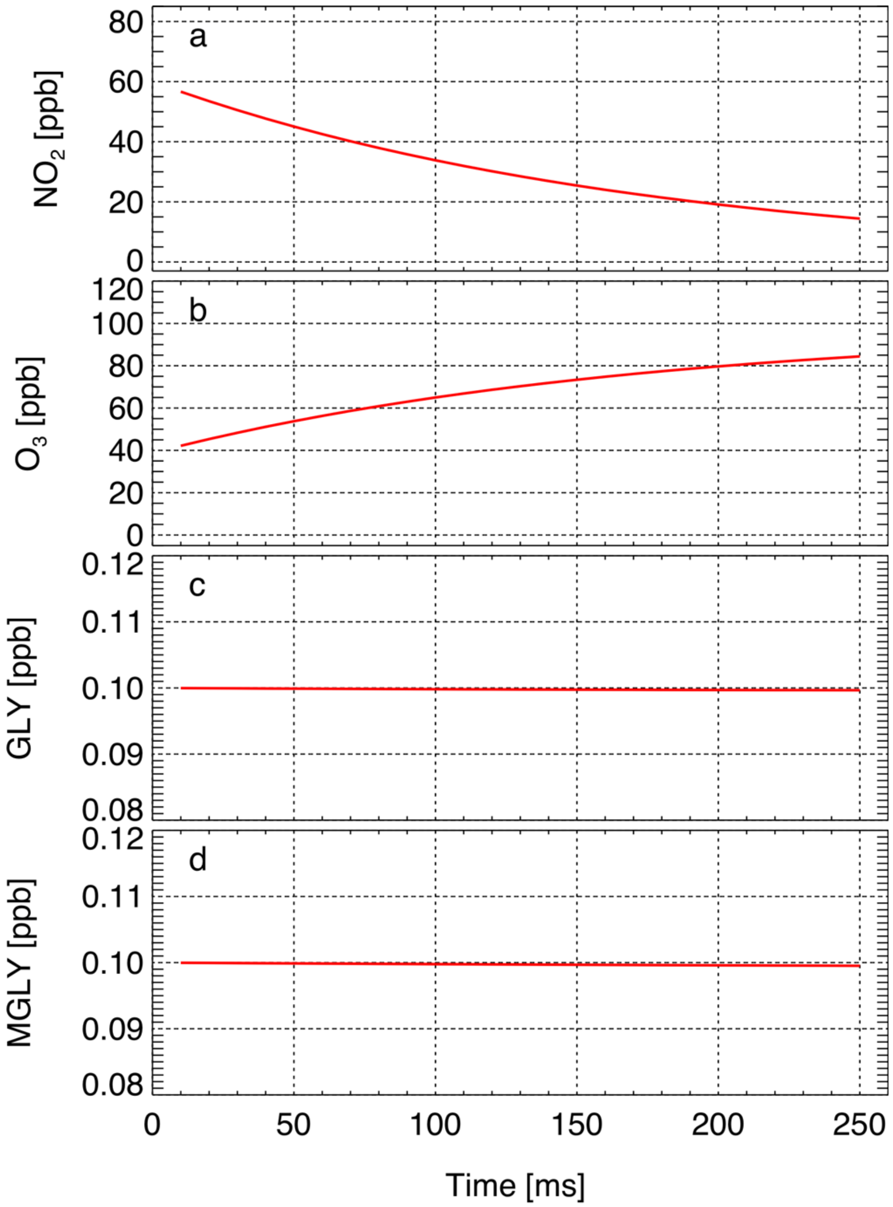

Figure S2. Model calculated concentrations of NO_2 (a), O_3 (b), GLY (c), and MGLY (d) in the photolysis cell of the NO_2 convertor. Note that the concentrations at 250 ms represent the condition of the sampled air exits the cell, since the residence time in the cell is about 250 ms.

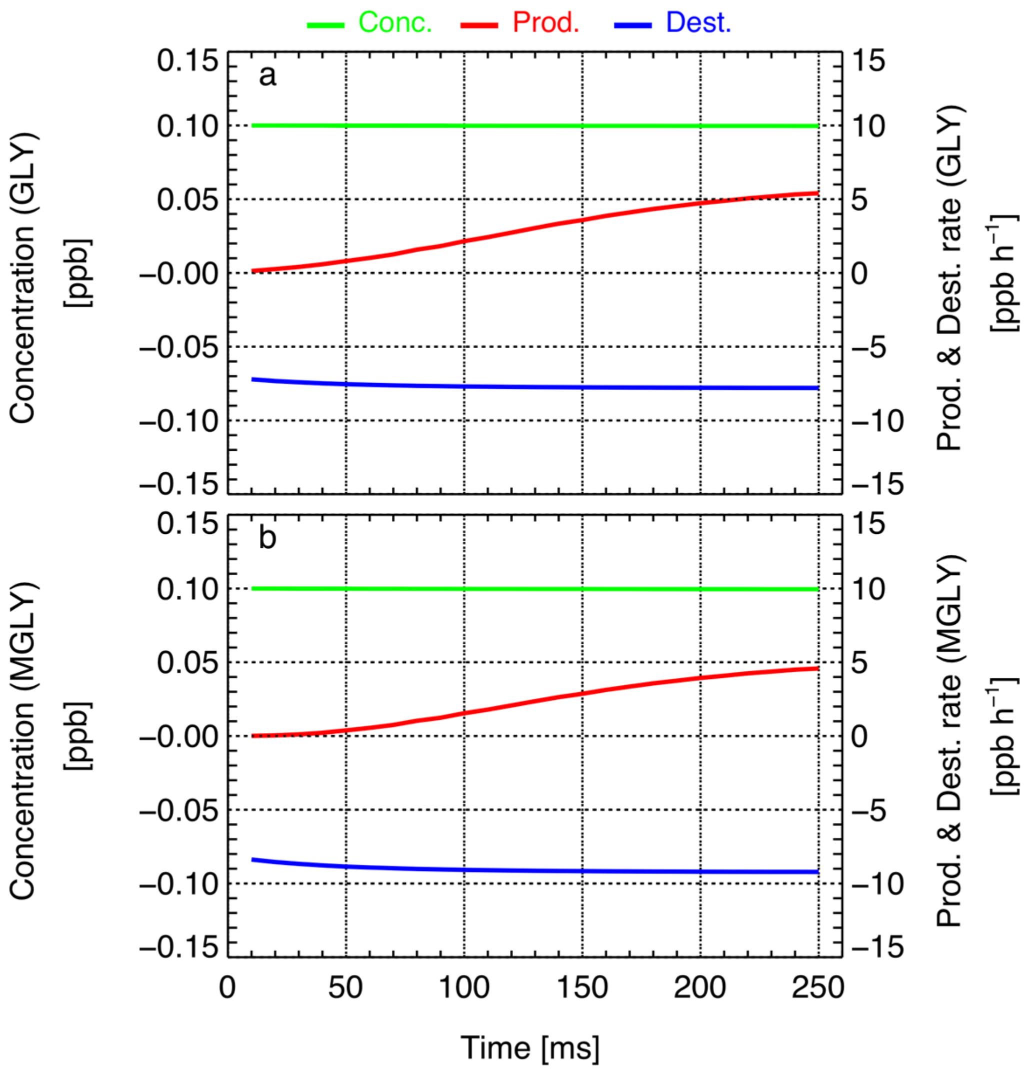

Figure S3. Model calculated concentrations (green), production rates (red), and destruction rates (blue) of GLY (a) and MGLY (b) in the photolysis cell of the NO_2 convertor. Note that the concentrations at 250 ms represent the condition of the sampled air exits the cell, since the residence time in the cell is about 250 ms.

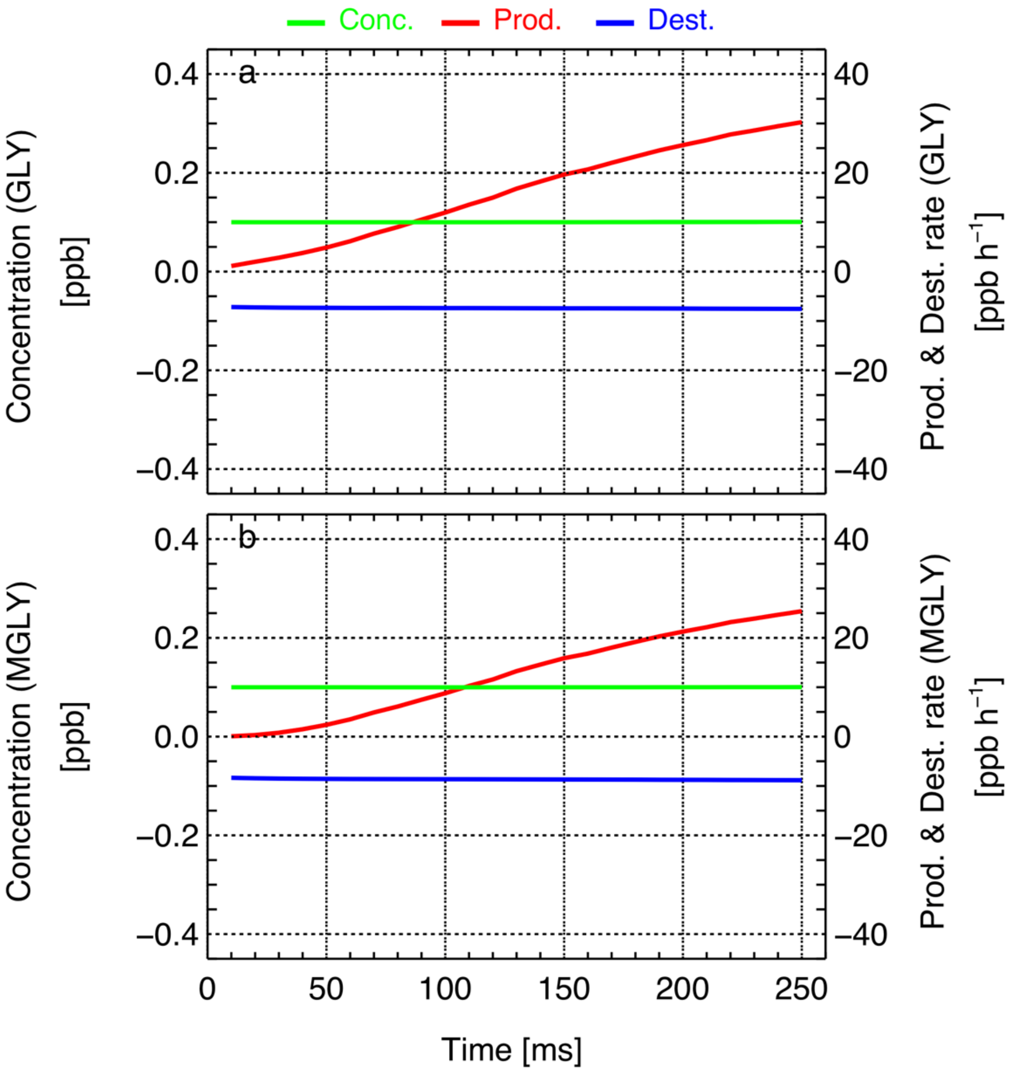

Figure S4. Model calculated concentration (green), production rate (red), and destruction rate (blue) of GLY (a) and MGLY (b) in the photolysis cell of the NO_2 converter. The initial concentrations of NMHCs in the model are set to 10 times of the values listed in Table 1. Note that the concentrations at 250 ms represent the condition of the sampled air exits the cell, since the residence time in the cell is about 250 ms.

An IBBCEAS system for atmospheric measurements of glyoxal and methylglyoxal in the presence of high NO_2 concentrations

Jingwei Liu[1,3], Xin Li[1,2,3], Yiming Yang[1,3], Haichao Wang[1], Yusheng Wu[1,*], Xuewei Lu[4], Mindong Chen[2], Jianlin Hu[2], Xiaobo ~~Fan~~[3]Fan[5], Limin Zeng[1,3], and Yuanhang Zhang[1,3]

~~[1]State~~[1] State Key Joint Laboratory of Environmental Simulation and Pollution Control, College of Environmental Sciences and Engineering, Peking University, Beijing, 100871, China P. R.
~~[2]Collaborative~~[2] Collaborative Innovation Centre of Atmospheric Environment and Equipment Technology, Nanjing University of Information Science & Technology, Nanjing, 210044, China P. R.
~~[3]Quadrant~~[3] International Joint Laboratory for Regional Pollution Control, Ministry of Education, Beijing, 100816, China P. R.
[4] State Key Laboratory for Structural Chemistry of Unstable and Stable Species, Institute of Chemistry, Chinese Academy of Sciences, Beijing 100190, P. R. China
[5] Quadrant Space (Tianjin) Technology Co., LTD, Tianjin, 301700, China P.R.
[*] Now at: Department of Physics, University of Helsinki, Helsinki, 00014, Finland

Correspondence to: Xin Li (li_xin@pku.edu.cn)

Abstract. A system based on incoherent broadband cavity enhanced absorption spectroscopy (IBBCEAS) has been developed for simultaneous measurement of nitrogen dioxide (NO_2), glyoxal (GLY) and methylglyoxal (MGLY). On this system, the measured light absorption ~~of light~~at around 460 nm is spectrally resolved. The concentration of absorbers is determined from a multi-component fit. At an integration time of 100 s, the measurement sensitivity (2σ) for NO_2, GLY, and MGLY ~~can reach~~is 18 ppt, 30 ppt, and 100 ppt, respectively. The measurement uncertainty which mainly originates from path length calibration, sampling loss, and uncertainty of absorption cross sections is estimated to be 8% for NO_2, 8% for GLY, and 16% for MGLY. When ~~applying~~deploying the instrument during field observations, we found significant influence of NO_2 on the spectra fitting for retrieving GLY and MGLY ~~concentration~~concentrations, which is caused by the fact that NO_2 has higher absorption cross section and higher ambient concentration. In order to minimize such an effect, a NO_2 photolytic convertor (NPC) which removes sampled NO_2 at an efficiency of 76% was integrated on the IBBCEAS system. Since sampled GLY and MGLY are mostly (⩾ 95%) conserved after passing through the NPC, the quality of the spectra fitting and the measurement accuracy of ambient GLY and MGLY ~~were~~could be largely improved.

1 Introduction

Glyoxal (CHOCHO, GLY) and methylglyoxal (CH_3COCHO, MGLY) are typical atmospheric α-dicarbonyl species that primarily enter the atmosphere through direct emissions from biomass burning and the oxidation of volatile organic compounds such as isoprene, aromatics, and alkenes (Fu et al., 2008). Therefore, GLY and MGLY are suitable indicators of

设置了格式: 上标
设置了格式: 上标
设置了格式: 上标
设置了格式: 上标

the atmospheric oxidation capacity (DiGangi et al., 2012). Atmospheric sinks of GLY and MGLY include photolysis and reactions with OH radicals (Volkamer et al., 2005a; Fu et al., 2008), which play an important role in the formation of both O_3 and peroxyacetyl nitrate (PAN) (Müller et al., 2016). Furthermore, the contribution of GLY and MGLY to the formation of second organic aerosol (SOA) has drawn widespread attention in the past few years (Washenfelder et al., 2011; Nakao et al., 2012; Meng et al., 2018). Although GLY and MGLY have relatively low molecular weights, they can form oligomers and participate in SOA formation in aqueous particles(Yu et al., 2011; Hamilton et al., 2013). In order to develop an in-depth understanding of the above processes, fast online measurements of GLY and MGLY with good sensitivity and accuracy are required.

Techniques for online measurements of GLY and MGLY can typically be categorized as methods based on either mass spectrometry or absorption spectroscopy. While proton transfer reaction time-of-flight mass spectrometry (PTR-ToF-MS) is considered to be a good mass spectrometry technique for measuring VOCs, its sensitivity is still too low to monitor the ambient concentration of GLY (Thalman et al., 2015; Stonner et al., 2017) and both $(H_2O)_3H_3O^+$ and acrylic acid ($C_3H_4O_2$) can interfere with MGLY results because they have the same *m/z* ratio (Thalman et al., 2015; Yuan et al., 2017; Zarzana et al., 2018). There are also many types of optical methods, including long path differential optical absorption spectroscopy (LP-DOAS) (Volkamer et al., 2005a), cavity-enhanced differential optical absorption spectroscopy (CE-DOAS) (Thalman and Volkamer, 2010), multi-axis differential optical absorption spectroscopy (MAX-DOAS) (Li et al., 2014), laser-induced phosphorescence (LIP) (Henry et al., 2012), incoherent broadband cavity enhanced absorption spectroscopy (IBBCEAS) (Min et al., 2016), and methods using satellite techniques like the global ozone monitoring experiment (GOME) (Vrekoussis et al., 2010) and ozone monitoring instrument (OMI) (Miller et al., 2014).

Since the first application of IBBCEAS by Fiedler (Fiedler et al., 2003), it has been widely used in laboratory studies and field campaigns to measure atmospheric trace gases such as H_2O, O_3, O_4, IO, I_2, OIO, SO_2, NO_2, NO_3, N_2O_5, HONO, HCHO, GLY, and MGLY (Vaughan et al., 2008; Washenfelder et al., 2008; Thalman and Volkamer, 2010; Axson et al., 2011; Kahan et al., 2012; Min et al., 2016; Wang et al., 2017; Duan et al., 2018). The core part of the instrument is a high-finesse cavity that holds of a pair of high-reflectivity mirrors, which typically have reflectivity greater than 0.9999. Because of the unmodulated broadband light source and multichannel detector, the concentrations of trace gases that have absorption structures can be determined simultaneously. Washenfelder et al. were the first to use this technology to measure GLY~~ and MGLY, and ~~. The precision (1σ) of their ~~IBBCEAS instrument has been used~~system is 29 ppt for ~~ground-based~~a 1 min sampling time (Washenfelder et al., 2008). Under the same time resolution, Thalman and Volkamer reduced the detection limit (2σ) to 19 ppt by using their LED-CE-DOAS (Thalman and Volkamer, 2010). The above two systems have been successfully applied to GLY measurements in field campaigns ~~and ~~(Washenfelder et al., 2011; Coburn et al., 2014). From aspects of miniaturization and improving time resolution, Min et al. optimized Washenfelder et al.'s IBBCEAS for aircraft ~~measurements (Washenfelder et al., 2008; Min et al., 2016).~~GLY measurements. The demonstrated precision (2σ) for retrievals of GLY is 34 ppt in 5 s (Min et al., 2016). The IBBCEAS developed by Fang et al. has a precision (1σ) of 28 ppt for GLY at 1 min averaging time. By applying Kalman filter to the retrieved concentrations, their measurement precision was improved to 8 ppt in 21 s (Fang et al., 2017). Within the range where GLY and MGLY have absorption structures, NO_2, H_2O, and O_4 also have structured absorptions; the spectra fitting and resultant concentrations of these α-dicarbonyl species may have interferences from NO_2 because NO_2 has a strong absorption structure between 430 nm to 470 nm and the ambient concentration of NO_2 is much higher than those of GLY and MGLY. Thalman et al. first encountered the challenge of fitting GLY and MGLY absorption spectra in the presence of high NO_2 concentrations (Thalman et al., 2015). ~~To our knowledge, an effective method has not yet~~ Liang et al. thought that the interference was caused by the accuracy of the convoluted NO_2 absorption cross section and tried to solve this problem by measuring NO_2 cross section with their own spectrometer (Liang et al., 2019). In this case, the accuracy of the retrieved NO_2 and GLY concentrations will be dependent on the accuracy of the NO_2 cross section they measured.

In this study, we present an incoherent broadband cavity enhanced absorption spectroscopy system for measuring GLY and MGLY and we describe the instrumental setup in detail. Instrumental sample loss was systematically determined using a novel, self-developed standard gas generator to supply GLY and MGLY and by combining our IBBCEAS with a NO_2 photolytic converter developed in-house, laboratory tests and in situ measurements were performed to investigate the interference of NO_2 on spectra fitting and measurements of GLY and MGLY. The accuracy of GLY and MGLY measurements in the presence of high NO_2 concentrations are discussed in terms of both experimental results and spectral simulations.

2 Instrumental setup

Instruments used in this study include a multi-gas calibrator (146i, Thermo Fisher Scientific Inc., Waltham, MA, USA), a standard gas generator for GLY and MGLY, a NO_2 photolytic converter (NPC), and a IBBCEAS. The first two instruments were used to supply and maintain a constant concentration of gas mixture, i.e., NO_2 and either GLY or MGLY. The NPC was used to photolyze the majority of the NO_2 in the mixed gas and the IBBCEAS was used as the detector for the three gases. Besides the multi-gas calibrator, the other three instruments were developed in our laboratory. The optical layout, flow system, and operation of our IBBCEAS are described in Sect. 2.1 and the details of standard gas generator and NPC are described in Sects. 2.2 and 2.3.

2.1 IBBCEAS

2.1.1 Optical layout

The optical layout of the IBBCEAS system consists of a light source module, an optical cavity module, and a detection module. The core of the light source module is a single-color LED (M450D3, Thorlabs, Newton, NJ, USA), centered at 445 nm with a full width at half maximum (FWHM) of 18 nm. The LED is powered by a constant current source and fixed on a heat sink connected to a thermostat in order to minimize fluctuations of its operating current and operating temperature. By setting appropriate PID (Proportion Integration Differentiation) parameters of the thermostat, the operating temperature were stabilized at 27.0 ± 0.1 ℃, in order to reduce intensity drift and wavelength shift of the LED.

A schematic depiction of the main body of the optical cavity module, which consists of seven mounting plates and four stainless steel bearings, is shown in Fig. 1a. The mounting plates are used to fix optical components and the bearings are used to ensure the coaxiality of these components. The entire cavity module adopts the cage structure design to enhance the system stability; this design is more convenient for replacing parts and adjusting the optical path, which can improve system reproducibility. Light emitted from the LED is directed into the cavity module by an optical fiber (1606205, Avantes, Apeldoorn, The Netherlands) and before coupled to the cavity, the light is collimated by an achromatic lens (ACA254-030-A, Thorlabs, Newton, NJ, USA) with a 30.0 mm focal length, which is mounted on a XY translating mount (CXY1, Thorlabs, Newton, NJ, USA) to finely adjust its position in both the horizontal and vertical directions. Parallel light behind the lens is introduced into a high-finesse cavity formed by a pair of high-reflectivity mirrors (122330, Layertec GmbH, Mellingen, Germany) with a radius curvature of 1.0 m and a diameter of 25.0 mm. The distance between the mirrors is 84 cm and the reflectivity of the mirrors, which are each fixed on a customized adjusting rack to finely adjust their pitch and yaw, is reported to be greater than 0.9998 between 420 nm and 450 nm. There is a small hole in the adjusting rack for the purge gas to pass through and we typically use high purity nitrogen (> 99.999%) as the purge gas to protect the surface of mirrors. After passing through the cavity, light is focused by another achromatic lens (ACA254-050-A, Thorlabs, Newton, NJ, USA) with a 50.0 mm focal length and stray light behind this lens is eliminated by a bandpass filter (FF01-442/42-25, Semrock, New York, USA).

Light exits the cavity module through a fiber bundle (SR-OPT-8024, Andor Tech., Oxford Instruments, England) that is coupled to the detection module, which is a grating spectrometer with a charge-coupled device (CCD) detector (Shamrock 303i, Andor Tech., Oxford Instruments, England). The system uses 600 $l \cdot mm^{-1}$ diffraction gratings (500 nm blaze) centered at 450 nm with wavelength coverage from 380 nm to 519 nm; the width of entrance slit is 100 μm and the corresponding wavelength resolution is 0.47 nm, which is determined by fitting the narrow emission line of a mercury lamp (Hg-1, Ocean Optics, Dunedin, FL, USA) at 435.84 nm. When operating the CCD detector, it is cooled to -70 ℃ to prevent noise generated by dark current.

2.1.2 Flow system

As shown in Fig. 1, the IBBCEAS flow system includes an inlet tube, aerosol filter, optical cavity, temperature sensor, pressure sensor, rotary vane pump (50104, Thomas, Gardner Denver, Germany), rotameter, three mass flow controllers (MFCs), and three solenoid valves (6014, Bürkert, Ingelfingen, Germany). Since Teflon has the best GLY transmission efficiency (Min et al., 2016), the inlet tube, aerosol filter and optical cavity were all constructed from Teflon.

After ambient air enters the IBBCEAS system through the fluorinated ethylene propylene (FEP) inlet tube, there is a polytetrafluoroethylene (PTFE) filter (25 μm thickness, 4.6 cm diameter, 2.5 μm pore size, Typris, China) to remove ambient aerosols. Gas passed through the filter is directed into the PTFE optical cavity (40.0 mm O.D., 20.0 mm I.D.) and its temperature and pressure are measured by the sensors after the cavity. The mass flow controller and a rotary vane pump at the end of the flow system maintain a constant gas flow rate through the cavity: 2 L/min.

The solenoid valve separates a by-pass line, which includes a rotameter, that branches from the inlet tube in front of the PTFE filter; this by-pass line is closed unless a reference spectrum is to be measured. The two remaining MFCs are used to control the flow rate of the two purge lines, through which either nitrogen or helium can enter the cavity module depending on which line has been opened by the solenoid valve. All valves and MFC flow rates are set automatically. Further operational details are given in the following sections.

2.1.3 Operation

The operation of the IBBCEAS system can be divided into four working modes, as shown in Fig. 1: measuring the spectrum of nitrogen (N_2 mode), measuring the spectrum of helium (He mode), measuring reference spectra (Reference mode), and measuring sample spectra (Sample mode). The first two working modes are used to calculate the mirror reflectivity and the other two are used to calculate the concentrations of trace gases. The theoretical equations used for these calculations are given in Sect. 3.

The intensity of measured spectra take some time to stabilize when the gas in the cavity is switched from nitrogen to helium. The amount of time for intensity stabilization is inversely related to the helium flow rate into the cavity; we ~~investigated~~measured the time required for signal stabilization at five different helium flow rates~~ between~~: 100 mL/min~~ to ~~, 200 mL/min, 300 mL/min, 400 mL/min, and 500 mL/min~~ and measured the intensity at 450 nm (Fig. 2a).~~. In order to reduce signal stabilization time and minimize signal fluctuation, we set the flow rate to 400 mL/min as it takes 2 minutes to achieve a stable signal. The signal also needs time to stabilize when the gas in the cavity is switched from the reference gas to sample air; we investigated a series of NO_2 concentration gradients (105 ppb, 90 ppb, 70 ppb, and 50 ppb) as sample air to quantify this time. ~~The results shown in Fig. 2b indicate that at~~At least 20 s are required for four different ~~NO_2 ~~concentrations of NO_2 to reach steady state; therefore, we purged the cavity for 20 s when the system was switched between Reference mode and Sample mode. When operating our IBBCEAS system with the above settings, it typically takes 5 minutes to calibrate the reflectivity of the mirrors each day (2 min in N_2 mode, 3 min in He mode), 2 min per hour to measure reference spectra in Reference mode, and for the rest of the day the system is operated in Sample mode. Switching between the four working modes is done automatically by self-developed software. When the instrument is operating normally, the only thing that needs to be done manually is changing the aerosol filter every 12 or 24 hours (depending on the concentration of particles in the sample air).

2.2 Standard gas generator for GLY and MGLY

Based on the methods described in previous studies (Washenfelder et al., 2008; Stonner et al., 2017), we designed a standard gas generator that uses high purity nitrogen (>99.999%), mass flow controller (F-201EV-MAD-22-V, 5 slm, Bronkhorst, The Netherland), U-type tube, cold trap, on-off valves, three-way valves, mix chamber, pump (50358, Thomas, Gardner

Denver, Germany), and pure GLY or MGLY powder~~, as shown in Fig. 3.~~. Diagram of the standard gas generator can be found in the Supplement.. The monomeric GLY and MGLY purification methods are the same as those described in the previous literature (Washenfelder et al., 2008; Pang et al., 2014). The operation of the standard gas generator is divided into the following three steps: (1) Passing high purity nitrogen over monomeric GLY or MGLY in the cold trap and transporting gaseous GLY or MGLY into the mix chamber; the temperature of cold trap (-72 ℃) is achieved by mixing dry ice and ethanol. (2) Rotating the three way valves (V_1 and V_2) to make nitrogen enter the mix chamber directly to dilute gaseous GLY or MGLY. (3) Rotating the three way valves (V_3 and V_4) and opening valve (V_6) to connect the inlet and outlet of the mix chamber to the both ends of the air pump, which evenly mixes the GLY or MGLY with nitrogen. While the air pump material may absorb some GLY or MGLY, it does not affect the gas mixture in any way that will impair the subsequent experiments.

Compared to the methods that produce GLY or MGLY by either heating GLY trimer dihydrate powder or MGLY powder (Gen et al., 2018) or using a temperature-controlled Teflon bubbler filled with solution (Min et al., 2016; Zarzana et al., 2018), the standard gas produced by our generator is more stable and can be maintained at a relatively constant concentration; the 50 L mix chamber used in this study can provide a constant concentration of GLY or MGLY for approximately 20 min. Furthermore, our generator can produce GLY or MGLY concentrations on the order of ppt to ppm by adjusting the flow rate of the elution gas and the dilution ratio of the gas in the mix chamber. Results from several instrumental performance tests are recorded in Table 1. The concentrations of the fourth GLY test and second MGLY test are 0.93 ppb and 0.61 ppb, respectively, which are close to their concentrations in ambient air (Li et al., 2014; Shen et al., 2018). During 20 min of standard gas supplement, the standard deviation of each concentration test is much smaller than the uncertainty of our IBBCEAS system, which indicates that our standard gas generator can provide good stability and reliability.

2.3 NO_2 photolytic converter

The NO_2 photolytic converter is mainly comprised of a photolytic module, power control module, and temperature control module. The photolysis cell is a 60.0 mm tube (18.0 mm O.D., 13.4 mm I.D.). When the system is operating at a flow rate of 2 L/min, the residence time is about 0.25 s. The core of the photolytic module is a set of 160 small LEDs (2865 COB, FLEDA, Taiwan) with a central wavelength of 395 nm and typical irradiance of 2000 mW/cm^2. The instrumental stability of the photolytic module is maintained by operating the module at a constant current (2.5 ± 0.01 A) and a constant temperature (26.0 ± 0.1 ℃), which are controlled by the power module and temperature module, respectively. The NPC was first used as a part of a NO_2 measuring device that has been successfully deployed in many campaigns ~~(Tan et al., 2018)~~(Tan et al., 2018), and in this study, we use the NPC to remove NO_2 from the sample gas. Further details about the photolytic efficiency for NO_2, GLY, and MGLY are given in Sects. 4.2 and 4.3, respectively.

3 Data analysis

3.1 Determination of trace gas concentrations

The extinction coefficient, $\alpha(\lambda)$, accounts for absorption, Rayleigh scattering, and Mie scattering caused by gases and particles in the cavity and can be described mathematically as following Eq. (1):

$$\alpha(\lambda) = \left(\frac{I_0(\lambda)}{I_a(\lambda)} - 1\right) \cdot \left(\frac{1-R(\lambda)}{d} + \sigma_{\mathrm{Rayl}}(\lambda)\right) \cdot \frac{1}{d_{\mathrm{Ratio}}} , \qquad (1)$$

where λ is the wavelength of light, $I_0(\lambda)$ is the reference spectrum, $I_a(\lambda)$ is the sample spectrum, d is the cavity length, $R(\lambda)$ is the mirror reflectivity, $\sigma_{\mathrm{Rayl}}(\lambda)$ is the extinction due to Rayleigh scattering, and d_{Ratio} is the ratio of effective cavity length to physical cavity length. Since particles are filtered out by the aerosol filter, Mie scattering in the cavity is negligible and $\alpha(\lambda)$ can be simplified to Eq. (2):

$$\alpha(\lambda) = \sum_i^n \sigma_i(\lambda) \cdot n_i , \qquad (2)$$

where $\sigma_i(\lambda)$ and n_i are the absorption cross section and number density of the *i*th gas absorber, respectively.

According to Eq (1) and (2), the effective absorption cross section of each absorber is required in order to determine the number density. Therefore, high resolution absorption cross sections were obtained from the literature – NO_2 (Vandaele, 2002), GLY (Volkamer et al., 2005b), MGLY (Meller et al., 1991), H_2O (Rothman et al., 2005), O_4 (Thalman and Volkamer, 2013) – and the absorption cross sections of NO_2, GLY, MGLY, and H_2O were processed with the instrument function determined by the Fraunhofer structure of a measured solar spectrum (Kurucz et al., 1984). Compared to the few Hg lines emitted around 430 nm, the more Fraunhofer lines in the wavelength range of our interest (i.e., 440 – 460 nm) can be used to generate a wavelength-dependent instrument slit function which account for the change of spectral resolution over the CCD pixels. The absorption cross sections of NO_2, GLY, and MGLY before and after processing with the instrument function are shown in Fig. ~~4~~2. The blue, thick solid line in this figure is the reference spectrum of our IBBCEAS system, which overlaps the absorption structures of these three absorbers.

By using the $\alpha(\lambda)$ calculated by Eq. (1) and the absorption cross sections used in Eq. (2), the number density of the absorbers can be fitted simultaneously. The main algorithm of this fitting process is nonlinear least squares with a fifth-order polynomial to account for drift in light intensity and cavity throughput. All data processing was performed by DOAS Intelligent System (DOASIS) spectral fitting software (Kraus, 2006).

3.2 Mirror reflectivity and effective cavity length

In order to calculate $\alpha(\lambda)$ using Eq. (1), $R(\lambda)$ and d_{Ratio} must be accurately quantified. We used pure nitrogen (> 99.999%) and pure helium (> 99.999%), two gases with distinct Rayleigh scattering sections, to calibrate $R(\lambda)$ according to Eq. (3):

$$R(\lambda) = 1 - d \cdot \frac{I_{\mathrm{N2}}(\lambda) \cdot n_{\mathrm{N2}} \cdot \sigma_{\mathrm{Rayl,N2}}(\lambda) - I_{\mathrm{He}}(\lambda) \cdot n_{\mathrm{He}} \cdot \sigma_{\mathrm{Rayl,He}}(\lambda)}{I_{\mathrm{He}}(\lambda) - I_{\mathrm{N2}}(\lambda)} \qquad (3)$$

where d is the cavity length, $I_{\mathrm{N2}}(\lambda)$ is the spectrum obtained in N_2 mode, $I_{\mathrm{He}}(\lambda)$ is the spectrum obtained in He mode, $\sigma_{\mathrm{Rayl,N2}}(\lambda)$ is the Rayleigh scattering cross section of nitrogen (Sneep and Ubachs, 2005), $\sigma_{\mathrm{Rayl,He}}(\lambda)$ is the Rayleigh scattering cross section of helium (Rao, 1977), and n_{N2} and n_{He} are the number density of nitrogen and helium, respectively. The reflectivity calibration results ~~from~~and corresponding effective path length of our IBBCEAS system during a field observation campaign in ~~the~~ Yangtze River Delta (YRD) , China is shown in Fig. ~~5~~3. During the ~~YRD~~ campaign, the $R(\lambda)$ ~~peak~~ was 0.99993 at 439 nm and the total uncertainty of this result is 5% because of the uncertainty in the scattering cross sections of N$_2$ (Sneep and Ubachs, 2005). After the system running continuously for 36 days, the ~~relative~~ change of the reflectivity was ~~0.0005% which is much smaller than the uncertainty of the measurement results.~~ 5×10^{-6}.

Because of the continuous purge gas at both ends of the cavity during sampling, the effective length of the cavity is shorter than its physical length; thus, d_{Ratio} is less than 1.0. In order to determine d_{Ratio}, we measured three NO$_2$ concentrations in the cavity, which were prepared from a bottled standard (10.2 ppm NO$_2$) and diluted with high purity nitrogen (> 99.999%) in the multi-gas calibrator (146i). The NO$_2$ concentrations were measured with and without purge gas and denoted as C_{NO2}^{WP} and C_{NO2}^{WTP}, respectively. When calculating C_{NO2}^{WP} and C_{NO2}^{WTP} simultaneously with Eq. (1) and (2), we assume that d_{Ratio} is equal to 1.0. Under this assumption, C_{NO2}^{WP} is less than C_{NO2}^{WTP} when the same concentration of NO$_2$ is being measured because the effective length of the cavity is overestimated. The measurement results of C_{NO2}^{WP} and C_{NO2}^{WTP} ~~are shown~~can be found in ~~Fig. 6~~the Supplement, which illustrates that the $C_{NO2}^{WP}/C_{NO2}^{WTP}$ ratio ~~is constant at~~fluctuated around 0.89 ~~(blue line in Fig. 6)~~ for the three NO$_2$ concentrations. The only variable in Eq. (1) and (2) is *d*; therefore, the $C_{NO2}^{WP}/C_{NO2}^{WTP}$ ratio is equal to the d_{Ratio}. Because of the 4% uncertainty of the NO$_2$ absorption cross section (Vandaele, 2002) and 2% uncertainty of the NO$_2$ prepared by the 146i, the uncertainty of the d_{Ratio} is ~~approximately 4~~4.5%.

4 Results and discussion

4.1 Instrument performance

4.1.1 Limit of detection and uncertainty

The precision of the IBBCEAS system can be estimated by calculating the Allan deviation (Allan, 1966), which is an algorithm that is commonly used for optical cavity technology (Brown et al., 2002; Langridge et al., 2008; Duan et al., 2018). We continuously measured 13600 spectra in Reference mode over 4 hours and designated the average value of the first 100 spectra as I_0. The remaining 13500 spectra were averaged in sets of 2, 4, 6, …, and ultimately 6750. Since the integration time of each spectrum is 1.0 s, we obtained a time series, I_a, that contains 6750 spectra with 2.0 s integration time, 3375 spectra with 4.0 s integration time, and so forth up to 2 spectra with 6750 s integration time. A time series of α at 439 nm was calculated using Eq. (1) and its Allan variance was determined using Eq. (4):

$$\sigma_{A_\alpha}^2(t) = \frac{1}{2(n-1)} \sum_{i=1}^{n-1} [\alpha_{i+1}(t) - \alpha_i(t)]^2, \quad (4)$$

where t represents the integration time, n represents the number of time series, $\alpha_i(t)$ is the extinction coefficient at each integration time from $i = 1$ to $i = n$. The arithmetic square root of the $\sigma^2_{A_\alpha}(t)$, the Allan deviation $\sigma_{A_\alpha}(t)$, can be used to evaluate the instrumental precision.

The results plotted in Fig. ~~7~~4 illustrate that when the integration time is less than 100 s, the sensitivity of our instrument can be improved by increasing the integration time. The instrument has the best precision when the integration time is near 100 s, after which the Allan deviation increases with integration time because of the drift of the light source. When the integration time is 100 s, the limit of detection (LOD) can be estimated by calculating the standard deviation of each absorber concentration retrieved from the 135 averaged spectra. The LOD of our IBBCEAS system in 100 s is estimated to be 18 ppt for NO_2, 30 ppt for GLY, and 100 ppt for MGLY.

According to Gaussian error propagation, the uncertainty associated with measurements of gas absorbers can be estimated using the uncertainty of the absorber's $\sigma(\lambda)$, $R(\lambda)$, d_{Ratio}, temperature, and pressure. For our IBBCEAS system, the uncertainty of $R(\lambda)$ is 5%, which is dominated by the uncertainty of the scattering cross sections of N_2. The uncertainty of the d_{Ratio} is ~~approximately~~ 4.5% and those of temperature and pressure are each 0.5 %. The uncertainties of NO_2, GLY, and MGLY can be found in the literature and are 4% (Vandaele, 2002), 5% (Volkamer et al., 2005b), and 15% (Meller et al., 1991), respectively. Based on the above parameters, the accuracy of our IBBCEAS system is estimated to be ± 8 % for NO_2, ± 8 % for GLY, and ± 16 % for MGLY.

4.1.2 Sample loss

Based on the standard gas generator for GLY and MGLY described in Sect. 2.2, experiments investigating sample loss in the sampling line were performed as follows. First, four Teflon sampling lines with length equal to 1 m, 3 m, 5 m, and 7 m were prepared. Second, the IBBCEAS system and standard gas generator were connected using the 1 m sampling line and gas was pumped into the IBBCEAS system for measurement. Third, replace the sampling line every four minutes in the following order: 3 m, 5 m, 7 m, and 1 m. The experiment was done twice for each length of sampling line and the results are shown in Fig. ~~8a~~5a. The concentrations measured during the first set of experiments fluctuated near 1.06 ppb and the concentrations measured during the second set fluctuated near 0.60 ppb. The two sets of experimental results demonstrated that sample loss is negligible in sampling line when its length is less than 7 m. Similarly, experiments investigating sample loss in the filters was performed using four filters with different levels of cleanliness (see Fig. ~~8c~~5c). Filter #1 is a clean filter that has never been used and #2, #3, and #4 are used filters that were saved during field campaigns; the daily average concentrations of PM2.5 corresponding to these filters are 11 $\mu g/m^3$, 37 $\mu g/m^3$, and 83 $\mu g/m^3$, respectively. During the sample loss experiments, the length of sampling line between the IBBCEAS system and the standard gas generator was fixed at 1 m and change the filter at the end of the sampling line in the order of #1, #2, #3, #4, and #1. The concentration of GLY was constant, 0.55 ± 0.02 ppb, when using the different filters (see Fig. ~~8b~~5b).

The above experiments demonstrate that GLY sample loss is negligible in both the sampling line and filter of our IBBCEAS system, which is consistent with the results from previous studies (Washenfelder et al., 2008; Min et al., 2016). The results from previous studies indicate that MGLY is even less reactive than GLY as the effective Henry's law consistent of MGLY is much smaller than that of GLY (Betterton and Hoffmann, 1988) and the gas-particle partitioning constant for MGLY is at least 30 times lower than that of GLY (Kroll et al., 2005); therefore, any loss of MGLY to the sampling line and filter should also be negligible.

4.1.3 Interference of NO_2 on spectra fitting

An example of spectra fit for one measurement during the YRD campaign is shown in Fig. ~~9~~6. The air pollution events at this rural site are mostly dominated by biomass burning, so relatively high concentrations of GLY and MGLY were measured. The wavelength range that we chose for quantifying GLY and MGLY includes strong structured absorption of NO_2. Furthermore, the concentration of NO_2 in the troposphere is much higher than that of either GLY or MGLY, especially during the air pollution events in China; therefore, the presence of high NO_2 concentrations may affect the spectral fitting of GLY and MGLY. In order to verify this conjecture, we processed the data obtained during two campaigns as follows: we plotted the changes in NO_2 concentration and spectra fitting residual over time on the same graph to check whether they have the same general trend, normalized the NO_2 concentration and fitting residual, and performed correlation analysis. Figure ~~10a~~7a illustrates that the NO_2 concentration and fitting residual trends of the processed data from the YRD campaign are similar, especially when the mixing ratio of NO_2 is greater than 10 ppb. The fitting residual is approximately $3.0 \times 10^{-9}\ \text{cm}^{-1}$ when the NO_2 mixing ratio is approximately 50 ppb. The correlation coefficient (R^2) of these two normalized parameters is 0.949, which indicates very good agreement.

During the PKU campaign, we attached the NO_2 photolytic convertor (NPC), described in Sect. 2.3, to the front of our IBBCEAS instrument to reduce the concentration of NO_2 in the sampled gas; analysis of the experimental results are given in Fig. ~~10c~~7c and ~~10d~~7d. In addition to our IBBCEAS system, another instrument for measuring NO_2 (42i, Thermo Fisher Scientific Inc., Waltham, MA, USA) was deployed during this campaign. Figure ~~10c~~7c shows that the NO_2 concentration measured by our IBBCEAS system is much lower than that measured by the 42i when the NPC is being used. When using the NPC, the correlation coefficient of the NO_2 concentration and fitting residual drops to 0.88 and the fitting residual falls to $5.0 \times 10^{-10}\ \text{cm}^{-1}$ while the ambient NO_2 mixing ratio is still approximately 50 ppb. Based on the above analysis, high concentrations of NO_2 interfere with the spectral fitting and this interference can be reduced by using the NPC. A model simulation was performed to evaluate the NPC while sampling an atmospheric background with VOCs, which verified that the production of GLY and MGLY in the photolytic cell of the NPC was negligible. Details of the model simulation are available in the Supplement. The NO_2 conversion efficiency of the NPC and its effect on the measured GLY and MGLY concentrations will be discussed in the following sections.

4.2 GLY measurements

In order to determine the NO_2 removal efficiency of our NPC, we prepared a concentration gradient of NO_2 gas samples, which were produced from a bottled standard (10.2 ppm NO_2) and diluted with high purity nitrogen (> 99.999%) in the multi-gas calibrator; each NO_2 concentration was measured twice, with the NPC on and off. The measurement results are shown in Fig. ~~11a~~8a, which illustrates that the removal efficiency of the NPC is constant at~~ approximately~~ 76% for the different concentrations of NO_2. Stability tests of the instrument were also performed and indicate that the efficiency does not change over time on the scale of hours. The impact of the NPC on the measured GLY concentration was tested using a similar method wherein the constant concentration of GLY produced by the standard gas generator was the gas to be measured. Based on the results shown in Fig. ~~11b~~8b, the NPC also photolyzes a small fraction of the GLY (~~approximately~~ 5%). Therefore, when the NPC is working, the GLY concentration obtained by spectra fitting needs to be corrected by dividing by 95%.

When repeating the above experiments using well-mixed NO_2 and GLY as the gas to be measured, we observed an interesting phenomenon whereby the concentration of NO_2 dropped rapidly while the NPC was running and the concentration of GLY increased. After the NPC was turned off, the concentrations of the two compounds returned to the same levels as before the NPC was turned on (see Fig. ~~11c~~8c). We conducted another experiment to prove that this phenomenon was not accidental. First, we prepared standard GLY and NO_2 gases and stored them in separate PTFE bags. Second, we mixed the GLY and NO_2 standard and delivered it to the IBBCEAS system. Third, we fixed the concentration of GLY in the cavity and gradually reduced the concentration of NO_2. Based on the spectra fitting results (see Fig. ~~12a~~9a), the concentration of GLY increased as that of NO_2 decreased, although we manually reduced the NO_2 concentration without changing that of GLY. Therefore, there seems to be a competitive relationship between the spectra fitting of NO_2 and GLY.

In order to further verify the observed phenomenon, we attempted to generate spectra to simulate the experimental NO_2 and GLY gas tests. The spectra were created by the following steps: (1) Set the NO_2 concentration n_{NO_2} and GLY concentration n_{GLY} to the value to be studied and substitute n_{NO_2}, $\sigma_{NO2}(\lambda)$, n_{GLY}, and $\sigma_{GLY}(\lambda)$ into Eq. (2) to calculate $\alpha(\lambda)$, where $\sigma_{NO2}(\lambda)$ and $\sigma_{GLY}(\lambda)$ are the absorption cross sections of NO_2 and GLY after processing with the instrument function. (2) Take the spectrum obtained during the reference mode as $I_0(\lambda)$ and substitute $I_0(\lambda)$, $R(\lambda)$, d, $\sigma_{\mathrm{Rayl}}(\lambda)$, d_{Ratio}, and $\alpha(\lambda)$ calculated in step (1) into Eq. (1). As all the parameters except $I_a(\lambda)$ in Eq. (1) are already determined, $I_a(\lambda)$ can be yielded. (3) Add a set of random numbers between 100 and 1000 representing the noise of the system to the intensity corresponding to each wavelength of $I_a(\lambda)$; this range, 100 and 1000 counts, was used because it is close to the actual noise level of our IBBCEAS system. We set the concentration of GLY to 1 ppb and the concentration of NO_2 to 0, 15, 30, 45 ppb to generate a series of $I_a(\lambda)$, and then calculated the concentration of these two gas absorbers from the generated $I_a(\lambda)$. Results from the spectral simulations are shown in Fig. ~~12b.~~9b. The fitting residual increased from 4×10^{-10} to 2×10^{-9} as the NO_2 concentration increased. It can be found that the retrieved GLY concentration is lower than its setting value while vice versa for NO_2. This is consistent with the experimental results discussed above~~, and could be caused by the lack of Rayleigh scattering and Mie~~

~~scattering in these $I_a(\lambda)$ simulations or other unknown reasons.~~. Therefore, it is obvious that the spectral resolving of NO_2 and GLY is competing with each other. Since NO_2 has a higher ambient concentration and stronger absorption structure than GLY, the GLY concentration determined by IBBCEAS could be underestimated in the presence of NO_2 and the higher the NO_2 concentration, the greater the underestimation. ~~Because whether the random number can represent the noise of the whole system is uncertain, it is difficult to evaluate the uncertainty of the spectral simulation~~The uncertainty of simulation results is mainly caused by two reasons. (1) Random numbers could be not good enough to represent the actual noise of the whole system. Since the intensity of LED and the reflectivity of mirrors are not evenly distributed with the wavelength, the corresponding signal-to-noise ratios (SNR) are also different at different wavelength. As for our system, the SNR within 450-468 nm are higher than that at other wavelengths. If we only reduced the random number by 5 times within 450-468 nm and did not change that at other wavelengths, the fluctuation of the fitted GLY concentration was also reduced by 5 times. (2) The impact of Rayleigh scattering and Mie scattering are not explicitly considered during the simulation. In this case, whether polynomial should be added in the spectral fitting or not would be a problem. The retrieved GLY concentration by using a fifth-order polynomial was 20% higher than that without including polynomial. Therefore, this method is only suitable for qualitative analysis instead of quantitative analysis presently. Further research is required to modify or parameterize the underestimation of GLY concentration and correct the measured value to be closer to its true value in ambient air.

4.3 MGLY measurements

Compared to NO_2 and GLY, the absorption cross section of MGLY is less structured, which means it is difficult to accurately calculate its concentration using spectral fitting. As demonstrated by the results in Table. 1, the difference in the measured MGLY concentrations is greater than those of GLY although the GLY and MGLY standard gases were produced by the same method and measured using the same instrument. Hence, each step in the process of MGLY spectral fitting needs to be considered carefully.

Selecting reasonable spectral fit ranges is necessary in order to accurately fit the concentration of MGLY; we chose four spectral fit ranges based on the structure of the absorption cross section of MGLY: 440-451 nm, 445-453 nm, 440-453 nm, and 430-453 nm~~ (see Fig. 13a).~~. Each spectral fit range was used to fit two experimental sets of MGLY measurements and ~~the~~according results are ~~shown~~available in ~~Fig. 13b~~the Supplement. Although the MGLY concentrations were determined using the same experimental data, the fitting results from different spectral ranges varied greatly. The results of fit range (1) and fit range (3) are similar and the range of results of (3) is relatively smaller. Fit range (2) covers the narrowest wavelength range and the MGLY concentrations from (2) are discrete, especially when the mixing ratio of MGLY is approximately 4 ppb. In contrast, fit range (4) covers the widest wavelength range and its fitting results are not ideal enough, even accounting for negative values when MGLY concentration is low. Based on these results, we prefer to use fit range (3), which covers the wavelength range from 440 to 453 nm, to determine MGLY concentrations in our studies.

In order to study the effect of NO_2 on MGLY measurements, experiments similar to those described in Sect 4.2 were conducted. First, prepared MGLY standard gas was passed through the NPC and measured by the IBBCEAS instrument. The results in Fig. ~~14a~~10a show that the NPC has no effect on the measured concentration of MGLY, which is different from the effect of the NPC on GLY. However, a similar phenomenon was observed when we repeated the above experiments with a mixture of MGLY and NO_2 (see Fig. ~~14b~~10b); the concentration of NO_2 dropped immediately once the NPC was turned on and the concentration of MGLY increased slightly, which is the same phenomenon that was observed for GLY. These results suggest that the MGLY concentration determined by IBBCEAS could also be underestimated in the presence of NO_2.

Spectral simulations were also performed to investigate the accuracy of the measured MGLY concentrations in the presence of NO_2. We set the concentration of MGLY to 1 ppb and the concentration of NO_2 to 0, 5, 10, 15, 20, 25 ppb in order to generate a series of $I_a(\lambda)$ using the same algorithm as in Sect. 4.2. The results of the simulations are shown in Fig. ~~16c~~10c, which illustrates that as the concentration of NO_2 increases, the concentration of MGLY will be underestimated. Therefore, in the presence of high NO_2 concentrations, measured MGLY concentrations may be lower than the real concentrations.

4.4 Comparisons to existing instruments

Comparisons of our IBBCEAS system with other instruments which are able to ~~simultaneously~~ measure GLY ~~and~~or MGLY within a time resolution of 30 minutes were made in Table. 2. For the GLY measurement, ~~ACES~~IBBCEAS, PFBHA-GC-MS, LIP, and CE-DOAS are available with detection limit values of 11-75 ppt and for the MGLY measurement, PTR-ToF-MS, CE-DOAS, PFBHA-GC-MS are available with detection limit values of 22-185 ppt. Compared with the existing instruments, the ability of our IBBCEAS to detect GLY and MGLY is comparable. From a comprehensive perspective, the new IBBCEAS has a good performance and can be used to simultaneously measure the concentration of GLY and MGLY in the atmosphere.

~~Compared with the ACES developed by Min et al., which is also be used to~~In addition to the new IBBCEAS system, there are four IBBCEAS reported to be able to measure GLY (Washenfelder et al., 2008; Min et al., 2016; Fang et al., 2017; Liang et al., 2019). As is shown in Table. 2, the detection limit of our system is slightly lower than that of Liang et al.'s and higher than that of Washenfelder et al.'s and Fang et al.'s. Compared with the IBBCEAS developed by Min et al., which is also be used to simultaneously measure GLY and MGLY (Min et al., 2016), under the same integration time (100 s), the Allan deviation of ~~their system (about 1.5 × 10^{-10} cm^{-1}) is higher than that of our system (8.4 × 10^{-11} cm^{-1}), which indicates that the IBBCEAS developed by us has a better instrumental precision and stability. With respect to the measurement interference of NO_2, existing CEAS do not have a good method to solve the problem.~~our system (8.4×10^{-11} cm^{-1}) is comparable to that of their system (about 7.5×10^{-11} cm^{-1}), which indicates that the IBBCEAS developed by us also has a good instrumental precision and stability. However, the volume of our IBBCEAS is at least twice as large as their system, and the time resolution is lower than theirs. So the IBBCEAS system developed by them will be a better choice for aircraft measurements. With respect to the measurement interference of NO_2, Liang et al. tried to solve this problem by measuring NO_2 cross section with their own spectrometer. This method improved the spectral fitting results and reduced the fitting residual by 33% (Liang et al., 2019). . For the IBBCEAS used by Thalman et al., the systematic bias was characterized as ~ 1ppt GLY/ppb NO_2, and ~ 5 ppt MGLY/ppb NO_2. At low NO_2 concentration (below 10 ppb), the small effect on GLY and MGLY retrievals was unnoticeable (Thalman et al., 2015). In contrast, before entering the cavity of our IBBCEAS, the NO_2 in sampled air is reduced by 76 %, so the systematic bias of our system caused by NO_2 can be reduced accordingly. Furthermore, during severe air pollution events, the NO_2 concentration in the optical cavity was always controlled between 10 and 20 ppb (see Fig. ~~10c),~~7c). When NO_2 concentration in ambient air was 50 ppb, the fitting residual can be reduced by 80%, which further ensures the minimization of NO_2 interference on measurements of GLY and MGLY.

5 Conclusions

We have developed and characterized an IBBCEAS instrument for simultaneously measuring NO_2, GLY, and MGLY in ambient air. Based on self-developed software, the entire system is highly automated; the only thing that needs to be done manually is replacing the particle filters during normal operation in field campaigns. Because of the uncertainties in the absorption cross sections, effective cavity length, and mirror reflectivity, the accuracies of the measured concentrations are estimated to be ± 8% for NO_2, ± 8% for GLY, and ± 16% for MGLY. Compared to IBBCEAS systems for the measurement of GLY and MGLY discussed in the existing literature, our novelties are mainly reflected in the following:

(1) A standard gas generator has been set up to provide a constant concentration of GLY or MGLY that can be maintained down to approximately 200 ppt, which is similar to their real concentrations in troposphere. The standard gas generator enables systematic experiments investigating sample loss and characterizing the IBBCEAS system.

(2) The interference of high NO_2 concentration on spectra fitting, and subsequently determining the concentrations of GLY and MGLY, is analyzed and discussed using both measured results and spectral simulations. In order to minimize the effect of NO_2 on GLY and MGLY, a NO_2 photolytic converter was used to remove NO_2 in the sampled air.

In summary, sample loss experiments with our IBBCEAS system demonstrated that sample loss of GLY and MGLY in the sampling line and particle filter are negligible. In terms of the interference of NO_2 on GLY and MGLY measurements, the spectral fit residual increases as the NO_2 concentration increases when all other conditions are the same. Furthermore, the measured GLY and MGLY may be underestimated in the presence of high NO_2 concentrations. By utilizing the NPC to remove sampled NO_2, the spectral fit residual is effectively reduced and the measured GLY and MGLY concentrations will be more accurate, such that the measured concentrations will be closer to their actual concentrations.

In order to accurately measure GLY and MGLY, the following methods could be developed to reduce the interference from NO_2. First, the sampled gas could be pre-treated to reduce the NO_2 concentration as much as possible without affecting GLY and MGLY. As discussed above, the higher NO_2 concentration, the greater underestimation of GLY and MGLY concentration, so reducing the NO_2 concentration can improve the accuracy of GLY and MGLY measurement results. The second method would be quantifying the competitive relationships in spectra fitting between NO_2 and both GLY and MGLY through laboratory experiments and theoretical calculations. After simultaneous retrieving concentrations of NO_2, GLY, and

MGLY, concentrations of GLY and MGLY could be corrected using the parametric relationship; however, because of the complexity of the actual atmosphere, parametric results obtained in the laboratory may not be able to be extended to field campaigns. The third option could be to develop a suitable method for removing only GLY and MGLY in sampled air and regard it as a new reference mode. By making the system switch between new reference mode and sample mode frequently, the spectra acquired in both modes will include the absorption of NO_2 and the spectra fitting will no longer be affected by NO_2. Unfortunately, such methods with sufficient specificity to selectively remove GLY and MGLY are not currently available. Moreover, the iterative algorithm used in CE-DOAS (Horbanski et al., 2019) could be helpful to accurately measure the concentration of the three at the same time.

Data availability.

The datasets used in this study are available from the corresponding author upon request (li_xin@pku.edu.cn).

Competing interests.

The authors declare that they have no conflict of interest.

Acknowledgements

This work was supported by the National Key R&D Program of China (2017YFC0209400) and by the National Natural Science Foundation of China (91644108). We thank Dr. Qingyu Liu ~~and Ms. Xuewei Lu~~ from Institute of Chemistry, Chinese Academy of Science for ~~their~~his help on purifying GLY and MGLY solid standards.

References

Allan, D. W.: Statistics of atomic frequency standards, Proceedings of the IEEE, 54, 221-230, 1966.

Axson, J., Washenfelder, R., Kahan, T., Young, C., Vaida, V., and Brown, S.: Absolute ozone absorption cross section in the Huggins Chappuis minimum (350–470 nm) at 296 K, Atmos Chem Phys, 11, 11581-11590, 2011.

Betterton, E. A. and Hoffmann, M. R.: Henry's law constants of some environmentally important aldehydes, Environ Sci Technol, 22, 1415-1418, 1988.

Brown, S. S., Stark, H., Ciciora, S. J., McLaughlin, R. J., and Ravishankara, A.: Simultaneous in situ detection of atmospheric NO 3 and N 2 O 5 via cavity ring-down spectroscopy, Review of scientific instruments, 73, 3291-3301, 2002.

Coburn, S., Ortega, I., Thalman, R., Blomquist, B., Fairall, C. W., and Volkamer, R.: Measurements of diurnal variations and eddy covariance (EC) fluxes of glyoxal in the tropical marine boundary layer: description of the Fast LED-CE-DOAS instrument, Atmos Meas Tech, 7, 3579-3595, 2014.

DiGangi, J. P., Henry, S. B., Kammrath, A., Boyle, E. S., Kaser, L., Schnitzhofer, R., Graus, M., Turnipseed, A., Park, J. H., Weber, R. J., Hornbrook, R. S., Cantrell, C. A., Maudlin, R. L., III, Kim, S., Nakashima, Y., Wolfe, G. M., Kajii, Y., Apel, E. C., Goldstein, A. H., Guenther, A., Karl, T., Hansel, A., and Keutsch, F. N.: Observations of glyoxal and formaldehyde as metrics for the anthropogenic impact on rural photochemistry, Atmos Chem Phys, 12, 9529-9543, 2012.

Duan, J., Qin, M., Ouyang, B., Fang, W., Li, X., Lu, K., Tang, K., Liang, S., Meng, F., Hu, Z., Xie, P., Liu, W., and Häsler, R.: Development of an incoherent broadband cavity-enhanced absorption spectrometer for in situ measurements of HONO and NO_2, Atmos Meas Tech, 11, 4531-4543, 2018.

Fang, B., Zhao, W., Xu, X., Zhou, J., Ma, X., Wang, S., Zhang, W., Venables, D. S., and Chen, W.: Portable broadband cavity-enhanced spectrometer utilizing Kalman filtering: application to real-time, in situ monitoring of glyoxal and nitrogen dioxide, Opt Express, 25, 26910-26922, 2017.

Fiedler, S. E., Hese, A., and Ruth, A. A.: Incoherent broad-band cavity-enhanced absorption spectroscopy, Chem Phys Lett, 371, 284-294, 2003.

Fu, T.-M., Jacob, D. J., Wittrock, F., Burrows, J. P., Vrekoussis, M., and Henze, D. K.: Global budgets of atmospheric glyoxal and methylglyoxal, and implications for formation of secondary organic aerosols, Journal of Geophysical Research, 113, 2008.

Gen, M., Huang, D. D., and Chan, C. K.: Reactive Uptake of Glyoxal by Ammonium-Containing Salt Particles as a Function of Relative Humidity, Environ Sci Technol, 52, 6903-6911, 2018.

Hamilton, J. F., Baeza-Romero, M. T., Finessi, E., Rickard, A. R., Healy, R. M., Peppe, S., Adams, T. J., Daniels, M. J., Ball, S. M., and Goodall, I. C.: Online and offline mass spectrometric study of the impact of oxidation and ageing on glyoxal chemistry and uptake onto ammonium sulfate aerosols, Faraday discussions, 165, 447-472, 2013.

Henry, S. B., Kammrath, A., and Keutsch, F. N.: Quantification of gas-phase glyoxal and methylglyoxal via the Laser-Induced Phosphorescence of (methyl)GLyOxal Spectrometry (LIPGLOS) Method, Atmos Meas Tech, 5, 181-192, 2012.

Kahan, T. F., Washenfelder, R. A., Vaida, V., and Brown, S. S.: Cavity-enhanced measurements of hydrogen peroxide absorption cross sections from 353 to 410 nm, The Journal of Physical Chemistry A, 116, 5941-5947, 2012.

Kraus, S.: DOASIS: A framework design for DOAS, Shaker, 2006.

Kroll, J. H., Ng, N. L., Murphy, S. M., Varutbangkul, V., Flagan, R. C., and Seinfeld, J. H.: Chamber studies of secondary organic aerosol growth by reactive uptake of simple carbonyl compounds, Journal of Geophysical Research: Atmospheres, 110, 2005.

Kurucz, R. L., Furenlid, I., Brault, J., and Testerman, L.: Solar flux atlas from 296 to 1300 nm, National Solar Observatory, 1984.

Langridge, J. M., Ball, S. M., Shillings, A. J., and Jones, R. L.: A broadband absorption spectrometer using light emitting diodes for ultrasensitive, in situ trace gas detection, Rev Sci Instrum, 79, 123110, 2008.

Li, X., Rohrer, F., Brauers, T., Hofzumahaus, A., Lu, K., Shao, M., Zhang, Y., and Wahner, A.: Modeling of HCHO and CHOCHO at a semi-rural site in southern China during the PRIDE-PRD2006 campaign, Atmos Chem Phys, 14, 12291-12305, 2014.

Liang, S., Qin, M., Xie, P., Duan, J., Fang, W., He, Y., Xu, J., Liu, J., Li, X., Tang, K., Meng, F., Ye, K., Liu, J., and Liu, W.: Development of an incoherent broadband cavity-enhanced absorption spectrometer for measurements of ambient glyoxal and NO_2 in a polluted urban environment, Atmos Meas Tech, 12, 2499-2512, 2019.

Meller, R., Raber, W., Crowley, J. N., Jenkin, M. E., and Moortgat, G. K.: THE UV-VISIBLE ABSORPTION-SPECTRUM OF METHYLGLYOXAL, Journal of Photochemistry and Photobiology a-Chemistry, 62, 163-171, 1991.

Meng, J., Wang, G., Hou, Z., Liu, X., Wei, B., Wu, C., Cao, C., Wang, J., Li, J., Cao, J., Zhang, E., Dong, J., Liu, J., Ge, S., and Xie, Y.: Molecular distribution and stable carbon isotopic compositions of dicarboxylic acids and related SOA from biogenic sources in the summertime atmosphere of Mt. Tai in the North China Plain, Atmos Chem Phys, 18, 15069-15086, 2018.

Michoud, V., Sauvage, S., Léonardis, T., Fronval, I., Kukui, A., Locoge, N., and Dusanter, S.: Field measurements of methylglyoxal using proton transfer reaction time-of-flight mass spectrometry and comparison to the DNPH–HPLC–UV method, Atmos Meas Tech, 11, 5729-5740, 2018.

Miller, C. E. S. C. C., Abad, G. G., Wang, H., Liu, X., Kurosu, T., Jacob, D. J., and Chance, K. V.: Glyoxal retrieval from the ozone monitoring instrument, 2014. 2014.

Min, K. E., Washenfelder, R. A., Dubé, W. P., Langford, A. O., Edwards, P. M., Zarzana, K. J., Stutz, J., Lu, K., Rohrer, F., Zhang, Y., and Brown, S. S.: A broadband cavity enhanced absorption spectrometer for aircraft measurements of glyoxal, methylglyoxal, nitrous acid, nitrogen dioxide, and water vapor, Atmos Meas Tech, 9, 423-440, 2016.

Müller, M., Anderson, B. E., Beyersdorf, A. J., Crawford, J. H., Diskin, G. S., Eichler, P., Fried, A., Keutsch, F. N., Mikoviny, T., and Thornhill, K. L.: In situ measurements and modeling of reactive trace gases in a small biomass burning plume, Atmos Chem Phys, 16, 3813-3824, 2016.

Nakao, S., Liu, Y., Tang, P., Chen, C. L., Zhang, J., and Cocker Iii, D. R.: Chamber studies of SOA formation from aromatic hydrocarbons: observation of limited glyoxal uptake, Atmos Chem Phys, 12, 3927-3937, 2012.

Pang, X., Lewis, A. C., Rickard, A. R., Baeza-Romero, M. T., Adams, T. J., Ball, S. M., Daniels, M. J. S., Goodall, I. C. A., Monks, P. S., Peppe, S., Ródenas García, M., Sánchez, P., and Muñoz, A.: A smog chamber comparison of a microfluidic derivatisation measurement of gas-phase glyoxal and methylglyoxal with other analytical techniques, Atmos Meas Tech, 7, 373-389, 2014.

Rao, A. P.: Absolute Rayleigh scattering cross sections of gases and freons of stratospheric interest in the visible and ultraviolet regions, 1977. 1977.

Rothman, L. S., Jacquemart, D., Barbe, A., Chris Benner, D., Birk, M., Brown, L. R., Carleer, M. R., Chackerian, C., Chance, K., Coudert, L. H., Dana, V., Devi, V. M., Flaud, J. M., Gamache, R. R., Goldman, A., Hartmann, J. M., Jucks, K. W., Maki, A. G., Mandin, J. Y., Massie, S. T., Orphal, J., Perrin, A., Rinsland, C. P., Smith, M. A. H., Tennyson, J., Tolchenov, R. N., Toth, R. A., Vander Auwera, J., Varanasi, P., and Wagner, G.: The HITRAN 2004 molecular spectroscopic database, Journal of Quantitative Spectroscopy and Radiative Transfer, 96, 139-204, 2005.

Shen, H., Chen, Z., Li, H., Qian, X., Qin, X., and Shi, W.: Gas-Particle Partitioning of Carbonyl Compounds in the Ambient Atmosphere, Environ Sci Technol, 52, 10997-11006, 2018.

Sneep, M. and Ubachs, W.: Direct measurement of the Rayleigh scattering cross section in various gases, J. Quant. Spectrosc. Radiat. Transf., 92, 293-310, 2005.

Stonner, C., Derstroff, B., Klupfel, T., Crowley, J. N., and Williams, J.: Glyoxal measurement with a proton transfer reaction time of flight mass spectrometer (PTR-TOF-MS): characterization and calibration, J Mass Spectrom, 52, 30-35, 2017.

Tan, Z., Rohrer, F., Lu, K., Ma, X., Bohn, B., Broch, S., Dong, H., Fuchs, H., Gkatzelis, G. I., Hofzumahaus, A., Holland, F., Li, X., Liu, Y., Liu, Y., Novelli, A., Shao, M., Wang, H., Wu, Y., Zeng, L., Hu, M., Kiendler-Scharr, A., Wahner, A., and Zhang, Y.: Wintertime photochemistry in Beijing: observations of ROx radical concentrations in the North China Plain during the BEST-ONE campaign, Atmos Chem Phys, 18, 12391-12411, 2018.

Thalman, R., Baeza-Romero, M., Ball, S., Borrás, E., Daniels, M., Goodall, I., Henry, S., Karl, T., Keutsch, F., and Kim, S.: Instrument intercomparison of glyoxal, methyl glyoxal and NO2 under simulated atmospheric conditions, 2015. 2015.

Thalman, R. and Volkamer, R.: Inherent calibration of a blue LED-CE-DOAS instrument to measure iodine oxide, glyoxal, methyl glyoxal, nitrogen dioxide, water vapour and aerosol extinction in open cavity mode, Atmos Meas Tech, 3, 1797-1814, 2010.

Thalman, R. and Volkamer, R.: Temperature dependent absorption cross-sections of O-2-O-2 collision pairs between 340 and 630 nm and at atmospherically relevant pressure, Phys Chem Chem Phys, 15, 15371-15381, 2013.

Vandaele, A. C.: High-resolution Fourier transform measurement of the NO2visible and near-infrared absorption cross sections: Temperature and pressure effects, Journal of Geophysical Research, 107, 2002.

Vaughan, S., Gherman, T., Ruth, A. A., and Orphal, J.: Incoherent broad-band cavity-enhanced absorption spectroscopy of the marine boundary layer species I 2, IO and OIO, Phys Chem Chem Phys, 10, 4471-4477, 2008.

Volkamer, R., Molina, L. T., Molina, M. J., Shirley, T., and Brune, W. H.: DOAS measurement of glyoxal as an indicator for fast VOC chemistry in urban air, Geophysical Research Letters, 32, 2005a.

Volkamer, R., Spietz, P., Burrows, J., and Platt, U.: High-resolution absorption cross-section of glyoxal in the UV–vis and IR spectral ranges, Journal of Photochemistry and Photobiology A: Chemistry, 172, 35-46, 2005b.

Vrekoussis, M., Wittrock, F., Richter, A., and Burrows, J.: GOME-2 observations of oxygenated VOCs: what can we learn from the ratio glyoxal to formaldehyde on a global scale?, Atmos Chem Phys, 10, 10145-10160, 2010.

Wang, H. C., Chen, J., and Lu, K. D.: Development of a portable cavity-enhanced absorption spectrometer for the measurement of ambient NO_3 and N_2O_5: experimental setup, lab characterizations, and field applications in a polluted urban environment, Atmos Meas Tech, 10, 1465-1479, 2017.

Washenfelder, R., Langford, A., Fuchs, H., and Brown, S.: Measurement of glyoxal using an incoherent broadband cavity enhanced absorption spectrometer, Atmos Chem Phys, 8, 7779-7793, 2008.

设置了格式: 下标

设置了格式: 下标

设置了格式: 下标

Washenfelder, R. A., Young, C. J., Brown, S. S., Angevine, W. M., Atlas, E. L., Blake, D. R., Bon, D. M., Cubison, M. J., de Gouw, J. A., Dusanter, S., Flynn, J., Gilman, J. B., Graus, M., Griffith, S., Grossberg, N., Hayes, P. L., Jimenez, J. L., Kuster, W. C., Lefer, B. L., Pollack, I. B., Ryerson, T. B., Stark, H., Stevens, P. S., and Trainer, M. K.: The glyoxal budget and its contribution to organic aerosol for Los Angeles, California, during CalNex 2010, Journal of Geophysical Research: Atmospheres, 116, 2011.

Yu, G., Bayer, A. R., Galloway, M. M., Korshavn, K. J., Fry, C. G., and Keutsch, F. N.: Glyoxal in aqueous ammonium sulfate solutions: products, kinetics and hydration effects, Environ Sci Technol, 45, 6336-6342, 2011.

Yuan, B., Koss, A. R., Warneke, C., Coggon, M., Sekimoto, K., and de Gouw, J. A.: Proton-Transfer-Reaction Mass Spectrometry: Applications in Atmospheric Sciences, Chem Rev, 117, 13187-13229, 2017.

Zarzana, K. J., Selimovic, V., Koss, A. R., Sekimoto, K., Coggon, M. M., Yuan, B., Dubé, W. P., Yokelson, R. J., Warneke, C., de Gouw, J. A., Roberts, J. M., and Brown, S. S.: Primary emissions of glyoxal and methylglyoxal from laboratory measurements of open biomass burning, Atmospheric Chemistry and Physics Discussions, doi: 10.5194/acp-2018-521, 2018. 1-35, 2018.

设置了格式: 字体: 10 磅

Table 1. Measurements of gaseous GLY and MGLY prepared by our standard gas generator and supplied for 20 min.

Species	Average concentration (ppb)	Standard deviation (ppb)
GLY	9.36	0.05
GLY	5.73	0.03
GLY	1.68	0.03
GLY	0.93	0.03
MGLY	3.99	0.10
MGLY	0.61	0.08

Table 2. Comparisons of the new IBBCEAS system with other instruments.

References~~Instrument~~	Method~~GLY Detection Limit (ppt)~~	Time resolution~~MGLY Detection Limit (ppt)~~	GLY Detection Limit (ppt)~~Time resolution~~	MGLY Detection Limit (ppt)~~References~~
This work~~IBBCEAS~~	~~18~~IBBCEAS	100 s	~~100 s~~30 (2σ)	100 (2σ)~~This work~~
Liang et al., 2019	IBBCEAS	30 s	23 (2σ)	Not mentioned
Michoud et al., 2018(Michoud et al., 2018)	PTR-ToF-MS	10 min	Not mentioned	22 (3σ)
Fang et al., 2017	IBBCEAS	1 min	28 (1σ)	Not mentioned
~~ACES~~Min et al., 2016	~~34~~IBBCEAS	5 s~~Not mentioned~~	~~5s~~34 (2σ)	~~Min et al., 2016~~Not mentioned
Pang et al., 2014~~PFBHA-GC-MS~~	PFBHA-GC-MS~~75~~	~~185~~30 min	~~30 min~~75 (2σ)	185 (2σ)~~Pang et al., 2014~~
~~PTR-ToF-MS~~	~~250~~	~~22~~	~~10 min~~	~~(Stonner et al., 2017; Michoud et al., 2018)~~
Henry et al., 2012~~LIP~~	~~11~~LIP	~~243~~5 min	~~5 min~~11 (3σ)	243 (3σ)~~Henry et al., 2012~~
~~CE-DOAS~~Thalman and Volkamer, 2010	~~19~~CE-DOAS	~~170~~1 min	~~1 min~~19 (2σ)	~~Thalman and Volkamer, 2010~~170 (2σ)
Washenfelder et al., 2008	IBBCEAS	1 min	29 (1σ)	Not mentioned
Volkamer, 2005a	LP-DOAS	2-15 min	150 (2σ)	Not mentioned

带格式的: 左, 行距: 1.5 倍行距
带格式的: 左, 行距: 1.5 倍行距
带格式表格
带格式的: 左
带格式的: 左, 行距: 1.5 倍行距
带格式的: 左
带格式的: 左, 行距: 1.5 倍行距
带格式的: 左, 行距: 1.5 倍行距
带格式表格
带格式的: 左
带格式的: 左, 行距: 1.5 倍行距
带格式的: 左, 行距: 1.5 倍行距
带格式的: 左
带格式的: 左, 行距: 1.5 倍行距
带格式的: 左, 行距: 1.5 倍行距
带格式表格
带格式的: 左
带格式的: 左, 行距: 1.5 倍行距
带格式的: 左, 行距: 1.5 倍行距
带格式的: 左
带格式的: 左, 行距: 1.5 倍行距

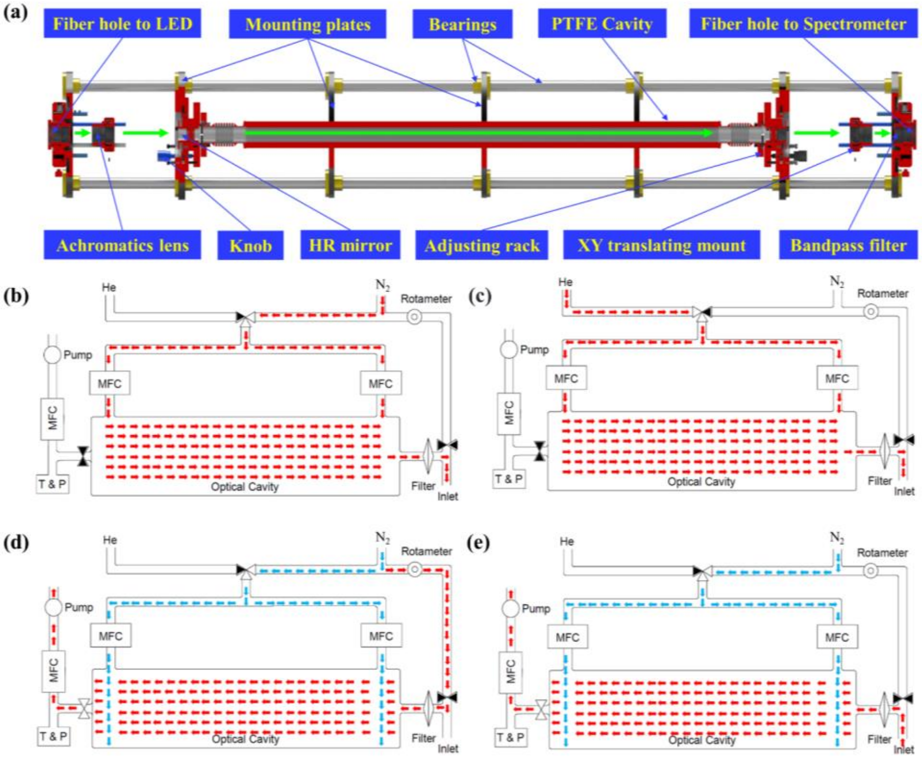
(a)
Fiber hole to LED
Mounting plates
Bearings
PTFE Cavity
Fiber hole to Spectrometer
Achromatics lens
Knob
HR mirror
Adjusting rack
XY translating mount
Bandpass filter
(b)
He
N_2
Rotameter
Pump
MFC
MFC
MFC
T & P
Optical Cavity
Filter
Inlet
(c)
He
N_2
Rotameter
Pump
MFC
MFC
MFC
T & P
Optical Cavity
Filter
Inlet
(d)
He
N_2
Rotameter
Pump
MFC
MFC
MFC
T & P
Optical Cavity
Filter
Inlet
(e)
He
N_2
Rotameter
Pump
MFC
MFC
MFC
T & P
Optical Cavity
Filter
Inlet

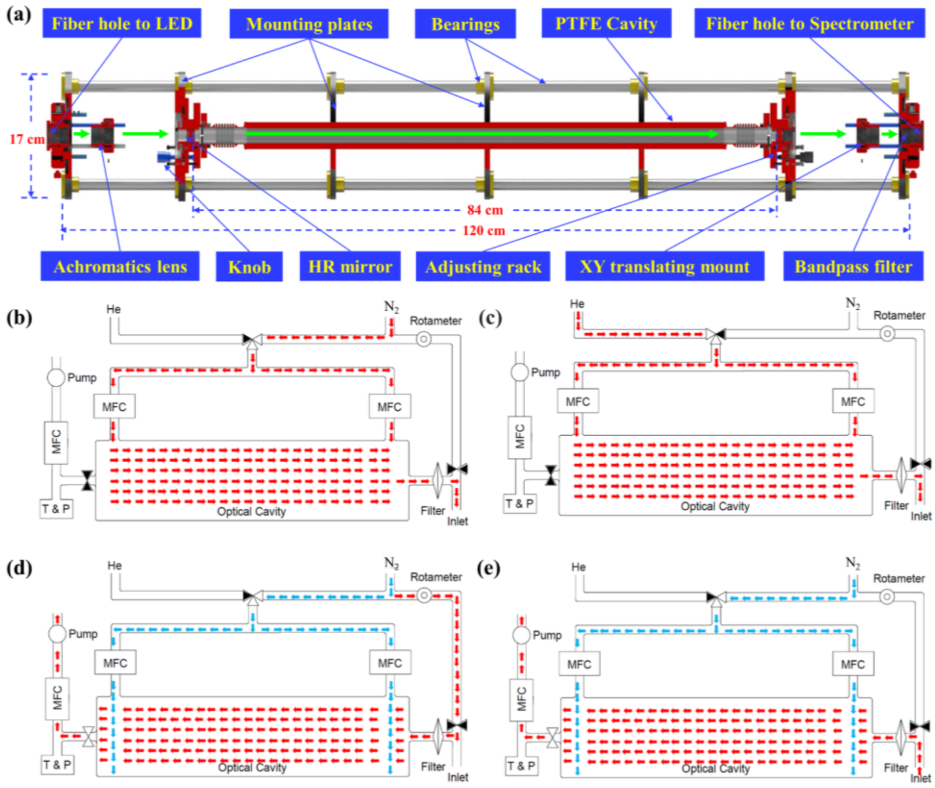

Figure 1. (a) Optical cavity module of the IBBCEAS system. Schematic layout of the instrumental flow system depicting four working modes: (b) N$_2$ mode; (c) He mode; (d) Reference mode; (e) Sample mode. The N$_2$ mode and He mode are used to calibrate mirror reflectivity and the Reference mode and Sample mode are used to calculate the concentrations of trace gases.

设置了格式: 字体: 小五, 加粗

设置了格式: 字体: 小五, 加粗

带格式的: 正文, 左

设置了格式: 字体: 小五

设置了格式: 字体: 小五

设置了格式: 字体: 小五

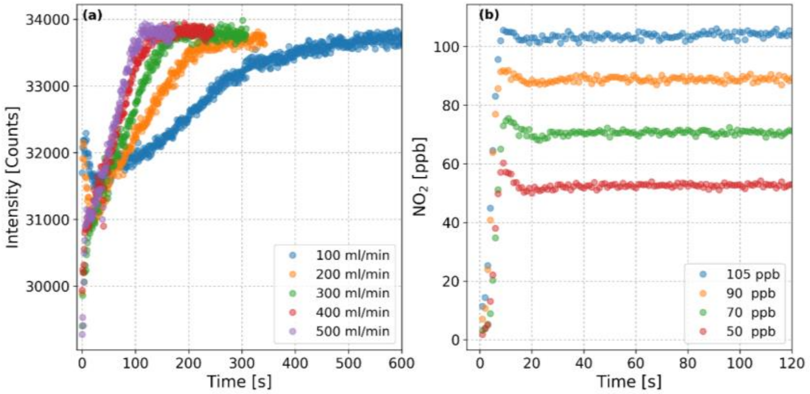

~~**Figure 2.** The time required to achieve a stable signal when switching between different working modes: **(a)** changes in intensity at 450 nm when switching from N_2 mode to He mode at different He flow rates; **(b)** changes in NO_2 concentration when switching from Reference mode to Sample mode with different NO_2 sample concentrations.~~

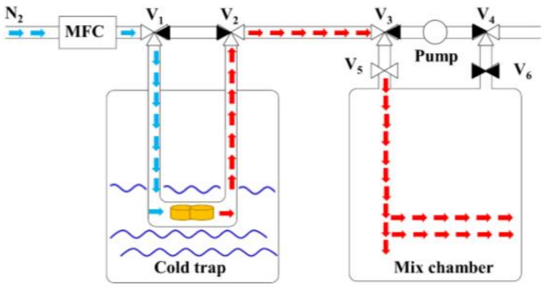

~~**Figure 3.** Diagram of the standard gas generator for GLY and MGLY.~~

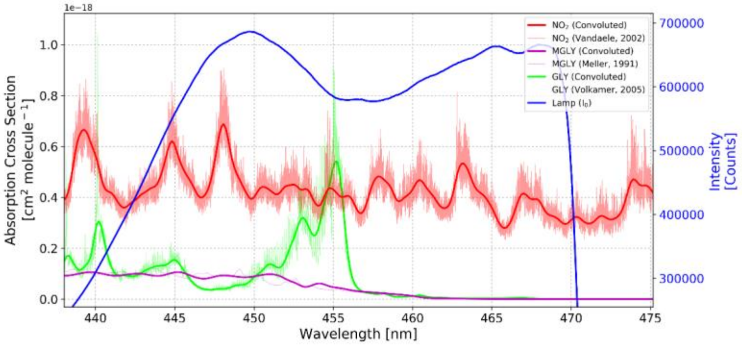1e−18
Absorption Cross Section
[cm² molecule⁻¹]
1.0
0.8
0.6
0.4
0.2
0.0
440
445
450
455
460
465
470
475
Wavelength [nm]
Intensity
[Counts]
700000
600000
500000
400000
300000
NO₂ (Convoluted)
NO₂ (Vandaele, 2002)
MGLY (Convoluted)
MGLY (Meller, 1991)
GLY (Convoluted)
GLY (Volkamer, 2005)
Lamp (I₀)

~~Figure 4.~~

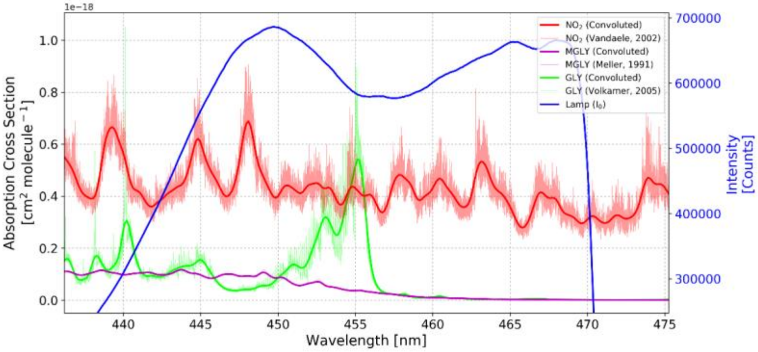

Figure 2. Reference spectrum of the IBBCEAS system (blue) and absorption cross sections of NO_2, GLY, and MGLY. The thin lines are the high resolution cross sections documented in the literature and the thick lines are the cross sections after processing with the instrument function determined by the Fraunhofer reference spectrum (Kurucz et al., 1984).

带格式的: 左, 行距: 1.5 倍行距

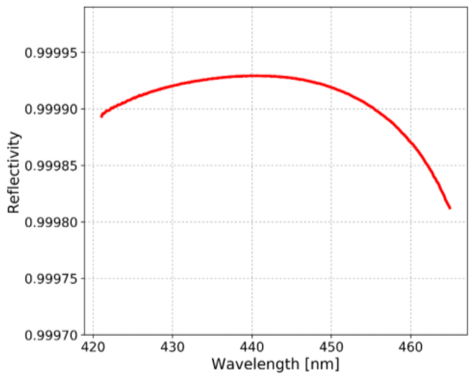

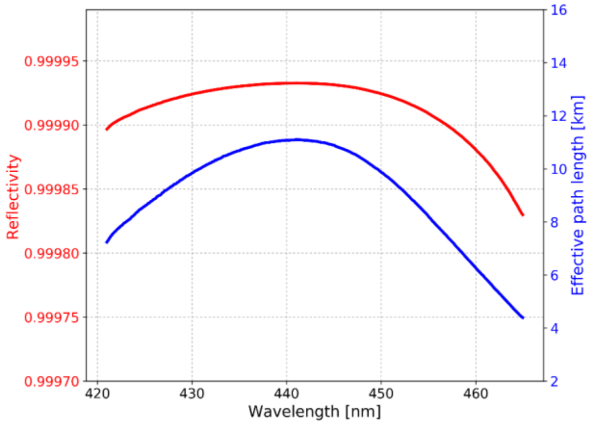

Figure ~~5~~3. Mirror reflectivity~~, $R(\lambda)$,~~ calibrated with high purity nitrogen (> 99.999%) and helium (> 99.999%) and corresponding effective path length during the YRD campaign.

带格式的: 左, 行距: 1.5 倍行距

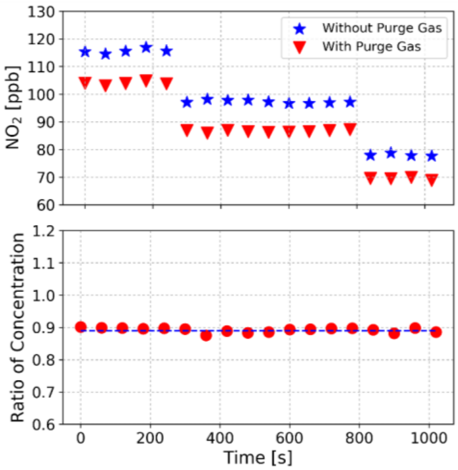

~~**Figure 6.** NO$_2$ concentrations measured with and without purge gas. The ratio of NO$_2$ concentration under different conditions is nearly constant at 0.89 (blue dotted line).~~

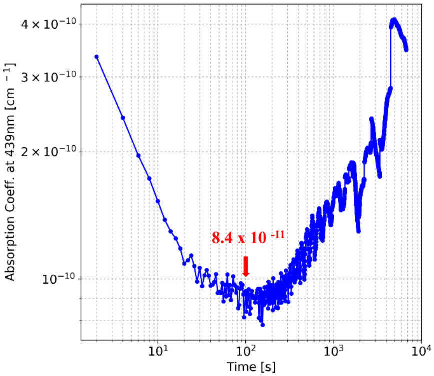
8.4 x 10 $^{-11}$
4×10^{-10}
3×10^{-10}
2×10^{-10}
10^{-10}
Absorption Coeff. at 439nm [cm $^{-1}$]
10^1
10^2
10^3
10^4
Time [s]

~~Figure 7.~~

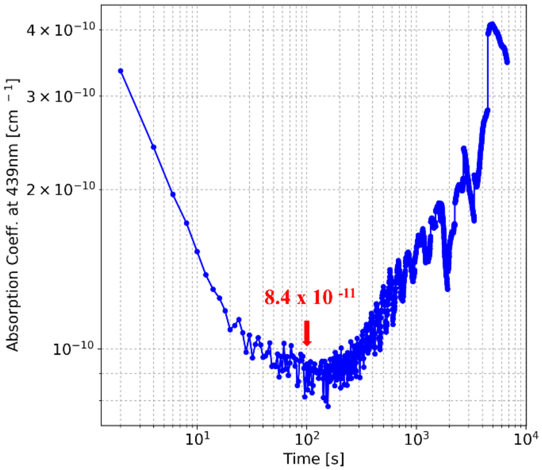

Figure 4. Allan deviation at 439 nm. The precision ($\mathbf{1\sigma}$) of the instrument is $\mathbf{8.4 \times 10^{-11}\ cm^{-1}}$ for an integration time of 100 s.

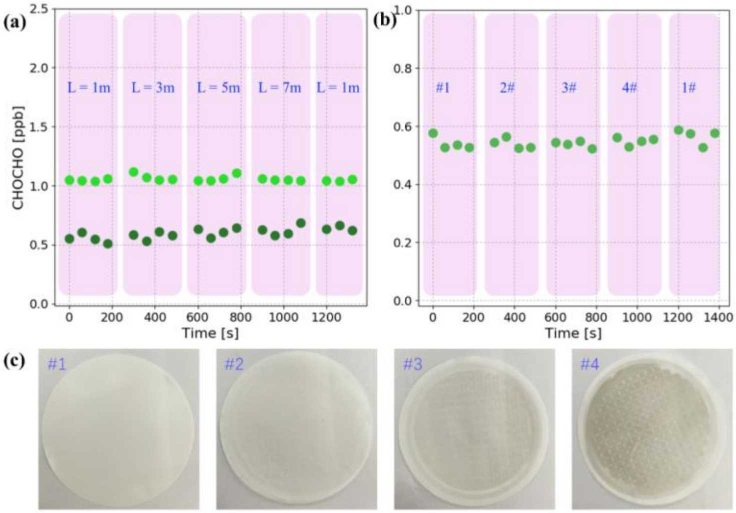

Figure ~~8~~5. Sample loss experiments: **(a)** Two sets of GLY concentrations (light green dots and dark green dots) measured with different lengths of sampling line (L). Each pink overlay represents the concentrations measured with the same length of sampling line; **(b)** GLY concentrations measured using particle filters with different levels of cleanliness~~.~~, which are marked as #1, #2, #3, and #4. Each pink overlay represents the concentrations measured with the same filter. (c) Samples of the four particle filters corresponding to (b); the daily average concentrations of PM2.5 corresponding to these filters are 0 $\mathbf{\mu g/m^3}$ (new filter), 11 $\mathbf{\mu g/m^3}$, 37 $\mathbf{\mu g/m^3}$ and 83 $\mathbf{\mu g/m^3}$, respectively.

带格式的: 两端对齐, 行距: 1.5 倍行距

设置了格式: 字体: 非加粗

设置了格式: 字体: 非加粗

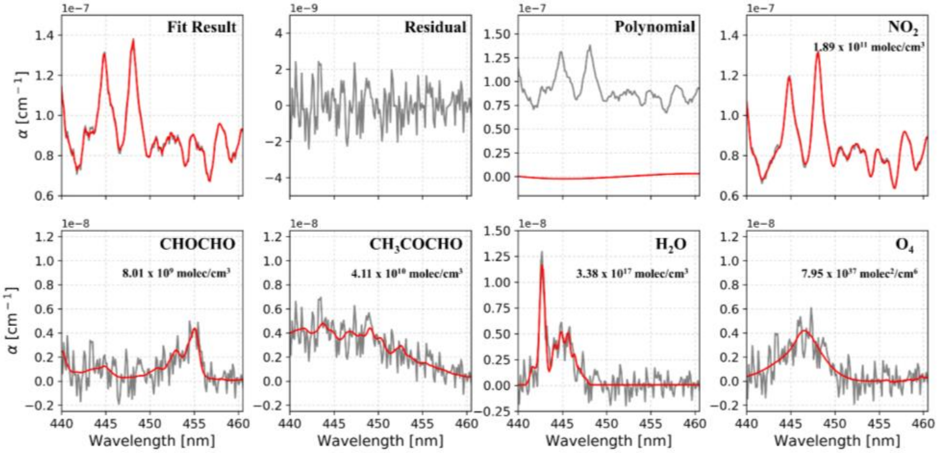

Figure ~~9~~6. An example of spectral fit for one ~~measurement~~spectrum (60s average) measured during the YRD campaign. Retrievals of NO_2, CHOCHO, CH_3COCHO, H_2O, and O_4 are shown, as well as the fifth-order polynomial, total fit, and residual. Red is the fitted spectrum and black is the fitted result plus residual.

带格式的: 左

设置了格式: 字体: 小五

设置了格式: 字体: 小五

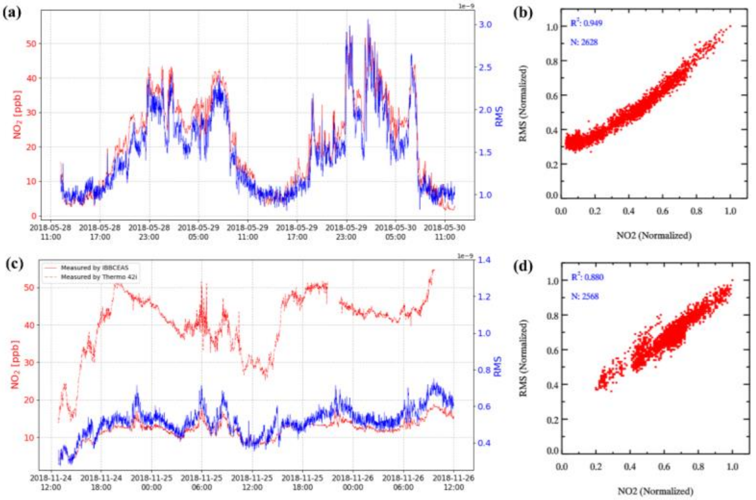
(a)
NO$_2$ [ppb]
RMS
1e−9
2018-05-28 11:00
2018-05-28 17:00
2018-05-28 23:00
2018-05-29 05:00
2018-05-29 11:00
2018-05-29 17:00
2018-05-29 23:00
2018-05-30 05:00
2018-05-30 11:00
(b)
R^2: 0.949
N: 2628
RMS (Normalized)
NO2 (Normalized)
(c)
Measured by IBBCEAS
Measured by Thermo 42i
NO$_2$ [ppb]
RMS
1e−9
2018-11-24 12:00
2018-11-24 18:00
2018-11-25 00:00
2018-11-25 06:00
2018-11-25 12:00
2018-11-25 18:00
2018-11-26 00:00
2018-11-26 06:00
2018-11-26 12:00
(d)
R^2: 0.880
N: 2568
RMS (Normalized)
NO2 (Normalized)

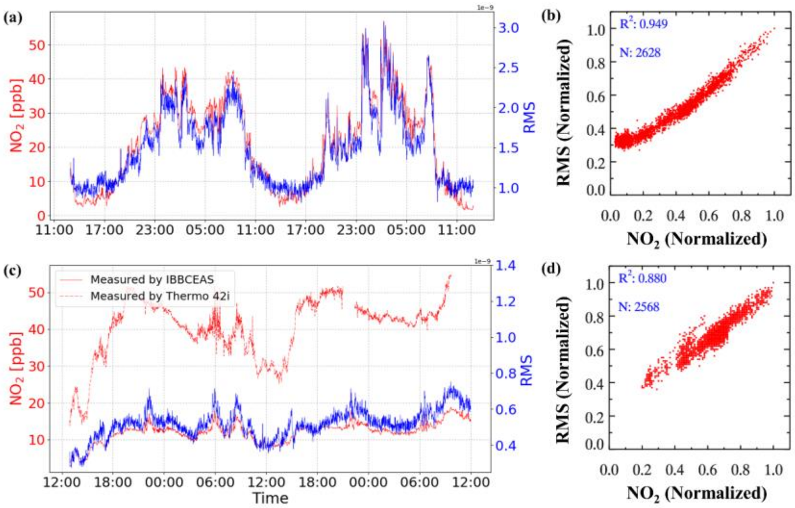

Figure ~~10~~7. (a) Time series and **(b)** correlation plot of NO_2 concentration and fitting residual from the YRD campaign. **(c)** Time series and **(d)** correlation plot of NO_2 concentration measured by IBBCEAS and fitting residual from the PKU campaign. The NO_2 concentration and fitting residual are normalized for comparison.

带格式的: 两端对齐, 行距: 1.5 倍行距

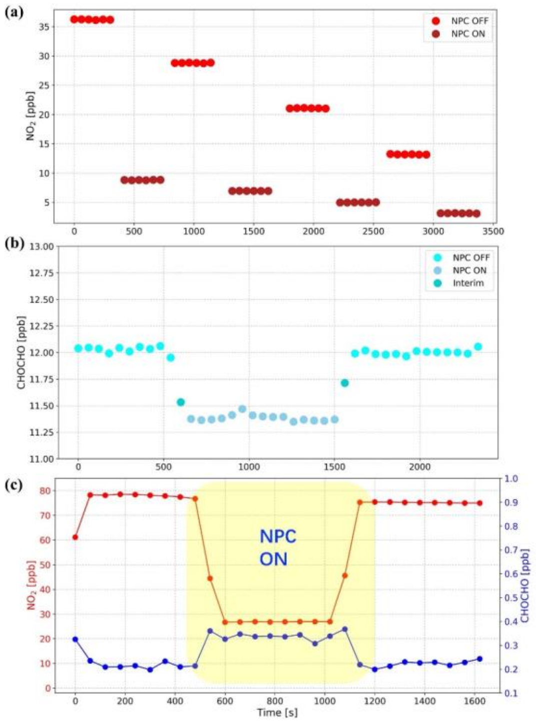

~~**Figure 11.** Results of photolysis experiments: **(a)** NO$_2$, **(b)** GLY, **(c)** well-mix NO$_2$ and GLY.~~

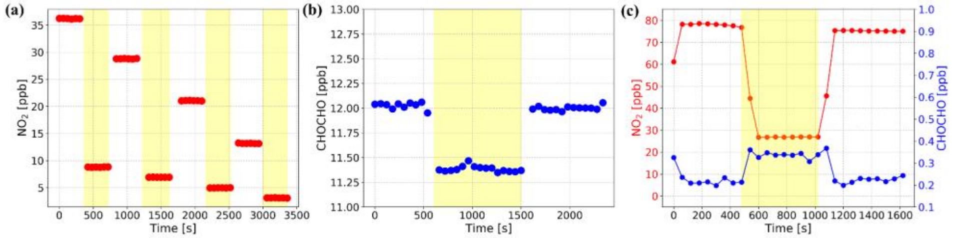

Figure 8. (a) NO_2 only test: A concentration gradient of NO_2 gas samples were measured twice, with the NPC on (yellow overlay) and off. The removal efficiency is constant at 76 % for different NO_2 concentrations. **(b)** GLY only test: The constant concentration of GLY produced by the standard gas generator was measured with the NPC on (yellow overlay) and off. A small fraction of the GLY (5%) was photolyzed by the NPC. **(c)** NO_2 and GLY mixture test: Well-mixed NO_2 and GLY was measured with the NPC on (yellow overlay) and off. The concentration of NO_2 dropped while the NPC was running and that of GLY increased. After the NPC was turned off, their concentrations returned to the same level as before the NPC was turned on.

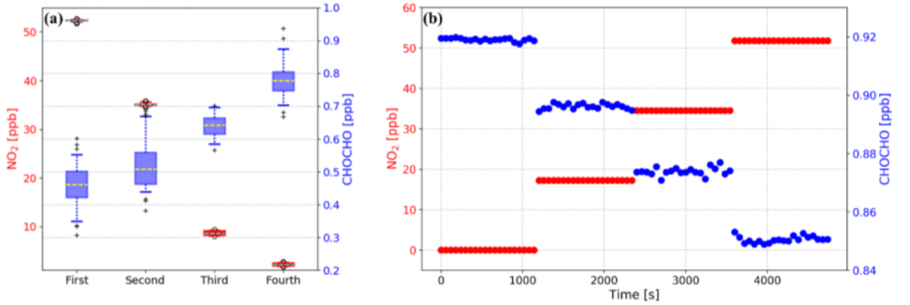

~~**Figure 12.** Impact of fixing the concentration of GLY and changing that of NO_2 on spectral fitting: **(a)** measurement results from the laboratory experiment; **(b)** results from the simulation experiment.~~

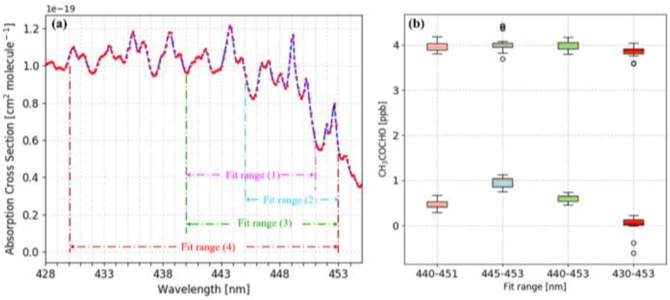

~~**Figure 13. (a)** Four spectral fit ranges for MGLY and **(b)** the corresponding concentrations of MGLY.~~

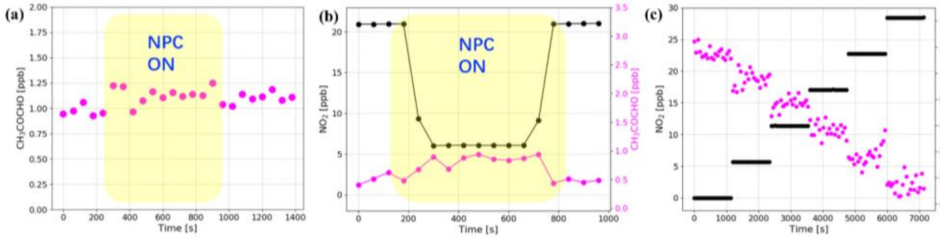

~~**Figure 14. (a)** Photolysis experiment of MGLY; **(b)** photolysis experiment of a MGLY and NO_2 mixture; **(c)** results from simulated spectra of a NO_2 and MGLY mixture.~~

Figure 9. (a) Keep the concentration of GLY constant and mix it evenly with different concentrations of NO_2 for four times. The concentration of GLY measured by IBBCEAS increased as that of NO_2 decreased, although only the NO_2 concentration was reduced manually. **(b)** Simulate a series of spectra with constant GLY concentration and increasing NO_2 concentration and then calculate concentrations of GLY and NO_2 by retrieving these simulated spectra. The retrieved GLY concentration decreased with the increasing NO_2 concentration, although the set value of GLY concentration in the simulation was kept constant.

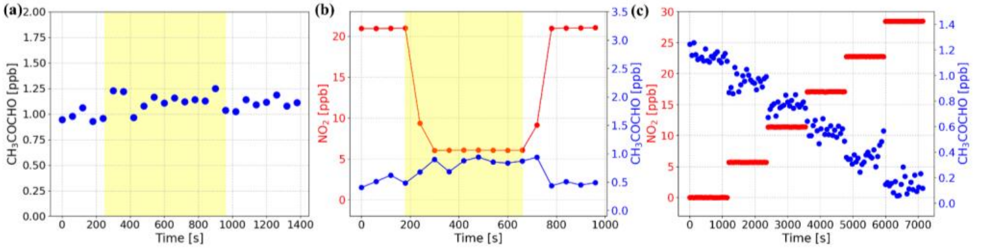

Figure 10. (a) The constant concentration of MGLY produced by the standard gas generator was measured with the NPC on (yellow overlay) and off. The effect of NPC on MGLY concentration is negligible. **(b)** Well-mixed NO_2 and MGLY was measured with the NPC on (yellow overlay) and off. The concentration of NO_2 dropped while the NPC was running and that of MGLY increased. After the NPC was turned off, their concentrations returned to the same level as before the NPC was turned on. **(c)** Simulate a series of spectra with constant MGLY concentration and increasing NO_2 concentration and then calculate concentrations of MGLY and NO_2 by retrieving these simulated spectra. The retrieved MGLY concentration decreased with the increasing NO_2 concentration, although the set value of MGLY concentration in the simulation was kept constant.